ABSTRACT

MPUNZA, HAPPINESS. Assessment of the Accuracy of Numerical Weather Prediction Models in Africa and South America Using Surface Observations. (Under the direction of Sandra Yuter).

The US National Oceanographic and Atmospheric Administration's (NOAA) Global Forecast Model (GFS) is a key asset for weather services world wide as it updates four times a day, produces hourly forecast output, and is freely available and accessible via the Amazon Web Services cloud. This study assesses GFS performance in predicting hourly air temperatures and dewpoints at 7 am local time (close to daily minimum temperature) and 3 pm local time (close to the daily maximum temperature) at 105 weather stations in Africa and 98 weather stations in South America, using hourly surface observations from December 2021 to November 2024. The accuracy of GFS forecasts for Africa and South America has not been previously systematically examined. The GFS ∼48 hour lead time forecast biases were analyzed seasonally and annually across seven simplified climate zones on both continents (Tropical, Dry, Mediterranean, Warm Wet Temperate, Cool Wet Temperate, Cold, and Polar). A key weakness of GFS revealed by this study is that the forecasts consistently underestimate dew points. Median annual dew point biases are too dry by $> 1°C$ across all climate zones at both 7 am and 3 pm local times and dry biases can exceed 4°C in specific locations seasonally. In comparison, air temperature forecasts are more reliable. The results can assist local forecasters to identify where the accuracy of the GFS model is limited and to apply regional and season-specific bias corrections as needed.

Assessment of the Accuracy of Numerical Weather Prediction Models in Africa and South America Using Surface Observations

by
Happiness Mpunza

A thesis submitted to the Graduate Faculty of
North Carolina State University
in partial fulfillment of the
requirements for the Degree of
Master of Science

Marine, Earth, and Atmospheric Science

Raleigh, North Carolina
2025

APPROVED BY:

Matthew Parker

Robert Mera

Sandra Yuter
Chair of Advisory Committee

BIOGRAPHY

Happiness Mpunza was born and raised in Dar es Salaam, Tanzania. She earned her B.S. in Meteorology from the University of Dar es Salaam, where her early interest in physics evolved into a passion for weather forecasting during an internship with a helicopter rescue startup operating on Mount Kilimanjaro. There, she began using weather models and ground observations to support complex rescue missions.

In 2019, she joined the Tanzania Meteorological Authority as a weather forecaster. In 2023, she moved to Raleigh, North Carolina, as a Fulbright Scholar to pursue a Master's degree in Atmospheric Sciences at North Carolina State University. After completing her studies, she looks forward to returning to Tanzania to continue her work in operational meteorology.

ACKNOWLEDGEMENTS

I am deeply grateful to Dr. Sandra Yuter for her guidance, support, and for helping me settle into North Carolina; these past two years were made easier because of her. I also thank the Environment Analytics Group, especially Dr. Matthew Miller, Warren Lewis, Laura Tomkins, and Cameron Gilbert, for their support with coding challenges related to bias calculations and data visualization. I would like to thank my committee members, Dr. Matthew Parker and Dr. Robert Mera for their valuable feedback and support throughout this research process. My Master's degree was fully funded by the Fulbright Program, whose support made this work possible.

Finally, a heartfelt thanks to my family, especially my husband, Bryton, for his unwavering emotional support and for being the primary parent of our son during this journey.

TABLE OF CONTENTS

LIST OF TABLES

LIST OF FIGURES

CHAPTER

1

INTRODUCTION

1.1 Motivation

The processes that determine day to day weather at any one location operate on a range of scales from local surface characteristics that can that vary at scales less than a few km to global circulations within the atmosphere and ocean. Weather services in several countries run operational forecasting models covering the entire globe in order to properly initialize numerical predictions for their specific regional areas of interest. The costs of the infrastructure (personnel and computers) to run an operational global weather model represent investments of the equivalent of millions of dollars. Weather services in countries that do not have the resources to run their own global models utilize available forecast model output provided by others.

The US National Oceanographic and Atmospheric Administration's (NOAA) Global Forecast Model (GFS) is a key asset for weather services world wide as it updates 4 times a day, produces hourly forecast output, and is freely available and accessible via the Amazon Web Services cloud. Since NOAA's mandate is to provide weather forecasts for the US, they have focused their model validation and refinement efforts on areas within the US as well as upstream locations such as the tropical Atlantic and tropical Pacific hurricane corridors (e.g. reports at https://www.emc.ncep.noaa.gov/users/meg/gfsv16/). We are not aware of any work examining biases in GFS forecasts for Africa or South America. Spot checks of time series of GFS forecasts versus observations for Africa and South America often show forecast errors of several °C (e.g. Fig. 1.1 and 1.2).

In practice, forecasters often devise adjustments to account for commonly occurring forecast biases for their domains of responsibility. For example, within the the Tanzania Meteorological Authority forecasters use a rule of thumb when interpreting the probabilistic output of the Global Ensemble Forecast System (GEFS). If the GEFS shows a probability of more than 25 mm in 24 hours (moderate rain), they adjust the forecast to at least 50 mm (heavy rain). Figure 1.3 shows an example of this type of adjustment and compares the predicted and observed precipitation amounts.

This study fills an important gap by examining the accuracy of GFS forecasts compared to surface observations over portions of the "global South", specifically the continents of Africa and South America. We follow methods developed as part of Patel et al. (2021) and Kennedy (2023) to assess 48-hour lead time forecasts from GFS compared to surface weather station observations. This study will examine three years of matched model-observation data to yield distributions of temperature and dewpoint biases across 105 stations in Africa and 98 stations in South America. The results of this analysis will aid users of GFS model output for Africa and South America to better understand its strengths and weaknesses.

1.2 Background: Environment Context for Africa and South America

Africa and South America feature climate and land cover types that differ from those in North America and Europe where global forecast models are typically evaluated (Fig. 1.4 and 1.5).

1.2.1 Climate Zones

Climate zones are an established method of grouping regions with similar climate that goes back to the ancient Greeks (Ahrens and Henson 2018). Vegetation cover is primarily controlled by annual temperature and precipitation variations and hence is an indirect means of grouping similar long term weather conditions. Vegetation-based climate zones are particularly useful for determining climate in regions that do not have routine weather observation records. One of the first widely used climate zones maps was first published by Köppen in 1900, well before daily weather observations were recorded in most of the world . Köppen's initial map has been updated several times as more weather data has become available worldwide. The Köppen-Geiger climate classification is now the common standard (Kottek et al. 2006). The 31 zones are defined based on temperature ranges as well as annual and seasonal precipitation (Kottek et al. 2006, their Table 1). For this analysis, we use a simplified version of the Köppen-Geiger map with 7 zones (Fig. 1.4, Gilbert, 2024, personal communication). By grouping GFS forecast errors by climate zone, we examine to what degree the model struggles in similar environments in both Africa and South America.

The particular spatial patterns of climate zones in Africa and South America (Fig. 1.6) are a result of interplay among topography, large scale subsidence versus rising motions, and prevailing winds by latitude for each continent (Fig. 1.7 and 1.8). There are large areas of the Tropical climate zone on both continents. Africa has a much larger region for the Dry climate zone than South America. The Mediterranean climate zone occurs along the northwestern edge of Africa and along a portion of the west coast of South America. South America has a large region of Warm, Wet Temperate climate east of the Andes between 20°S and 40°S. Africa has a smaller area of this climate zone centered near 20°S. The Cool, Wet Temperate, and Cold Dry climate zones occur in small patches on both continents.

Both Africa and South America straddle the equator making the Hadley Cells and the Intertropical Convergence Zone (ITCZ) (Fig. 1.9) the dominate large scale patterns influencing their weather except at the southern tips of each continent. The middle latitude portions of Africa and South America are influenced by midlatitude synoptic wave patterns. In the tropics, the seasonal shifts in the location of the ITCZ yield "rainy" and "dry" seasons (Fig. 1.10). Near the equator there are two rainy seasons corresponding to the times of the equinoxes in March and September. Tropical locations further from the equator have just one rainy season when the ITCZ is located overhead near the time of the June solstice for locations north of the equator, and near the time of the December solstice for locations to the south (Fig. 1.11).

1.2.2 West African Monsoon

The West African monsoon is a seasonal wind shift that drives the rainy season in West Africa from June to September. As a heat low develops over the Sahara, southerly winds bring moist air from the Gulf of Guinea toward the Sahel and act to intensify the ITCZ convergence compared to open ocean conditions (Fig. 1.12). The monsoon rainfall peaks when and where the near surface air contains the largest amount of combined heat and moisture (Biasutti et al. 2023). The timing of the monsoon is critical for agriculture, especially for small farmers in the Sahel along the southern edge of the Sahara. A delayed start or an early end to the rainy season can lead to crop failure, food insecurity, and economic loss. Regional rainfall patterns are closely linked to the position of the ITCZ, which responds to larger energy imbalances between the hemispheres. The timing and variability of monsoon rainfall is important context for how GFS temperature biases may differ between the wet and dry seasons.

1.2.3 El Nino Southern Oscillation (ENSO) phase

In comparison to Asia and Oceania, Africa and South America have smaller geographic areas that experience significant shifts in conditions as ENSO phase varies (Fig. 1.13). Over our three year study period from December 2021 to November 2024, the ENSO phase changed from a moderate La Nina (Dec 2021-Feb 2023) to a strong El Nino (June 2023-May 2024) then back to neutral conditions (June 2024-Nov 2024) (Table 1.1). In terms of this study, for Africa we expect the interannual variability among the three years to be largest in Dec 2023 - Feb 2024 when the El Nino was strong and broad geographic impacts over the continent are expected (Fig. 1.13). These impacts include wetter conditions in tropical eastern Africa and dry and warm conditions in southeast Africa. For Africa in JJA during El Nino the continent experiences little to no changes from ENSO neutral conditions. For South America, the strong El Nino conditions in JJA are expected to yield large areas with warm temperature anomalies along both coasts in tropical and subtropical latitudes, a small area of dry and warm conditions along the north edge of the continent and a small wet area along the midlatitude west coast. In DJF, the geographic region of warm conditions on the east coast of South America shrinks in area compared to El Nino in JJA and there is region of wet conditions to its south. Dry conditions are present along the northeast coast.

Portions of the analysis described in subsequent chapters examine bias statistics year by year as well by combining all three years together. On balance, the variations in ENSO phase over the 3 year study period did not yield large and significant differences in the distribution statistics.

Table 1.1: Oceanic Nino Index (ONI). Blue negative values indicate La Nina conditions and red positive values indicate El Nino conditions. Values between ±0.5 are neutral conditions. Note that DJF includes December from the previous year, e.g. 2022 DJF = December 2021 - February 2022. Source: NOAA Climate Prediction Center.

Year/Season	**DJF**	**MAM**	**JJA**	**SON**
2022	-1.0	-1.1	-0.8	-1.0
2023	-0.7	0.2	1.1	1.8
2024	1.8	0.7	0.0	-0.3

1.3 Goals

Previous work on assessing GFS forecast biases compared to surface observations by Patel et al. (2021) and Kennedy (2023) examined errors over North America. The lower spatial density of surface weather observations in Africa and South America as compared to North America, and the fact that many of the South American and some of the African stations do not transmit hourly data overnight constrained several aspects of the analysis (see Chapter 2). We focus on examining the distributions of biases for air temperature and dew point near the typical diurnal daily minimum temperatures at 7 AM local time and daily maximum temperature at 3 PM local time for the approximately 48-hour lead forecasts. Kennedy (2023) found that biases in these variables at 48-hour at lead times were similar to those at 36-hour and 24-hour lead times. Evaluation of air temperatures and dew points at 7 AM and 3 PM is relevant for a wide range of applications from human, animal and crop stresses to energy usage. *The goals of this analysis are to provide information on the relative reliability and typical bias values of the GFS forecasts for these local times over different seasons which will be of use to weather services in Africa and South America as well as to potentially motivate GFS model refinements.*

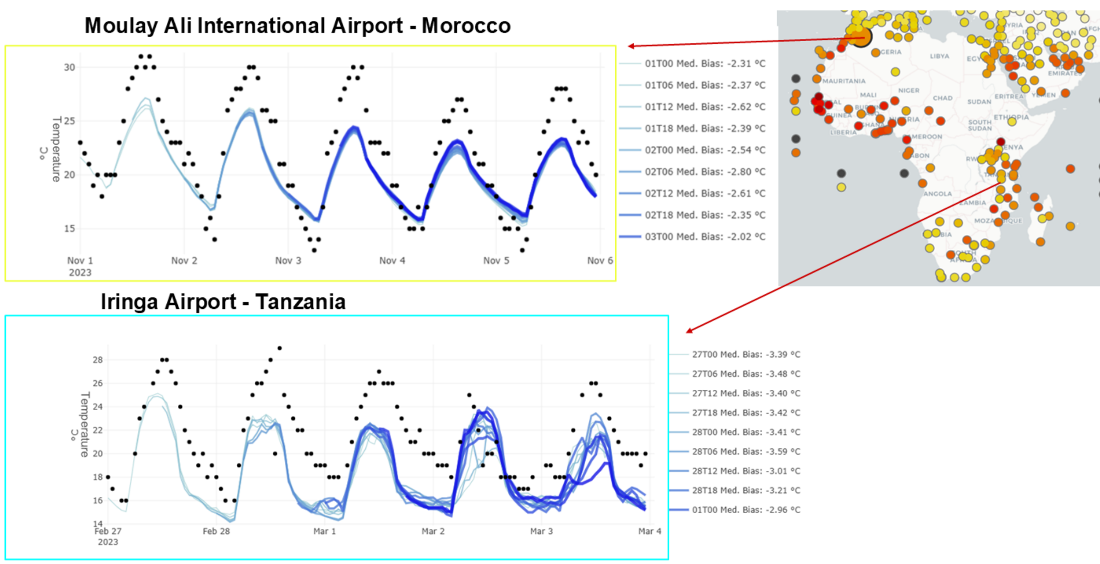

Figure 1.1: Time series of GFS temperature forecasts at Moulay Ali Airport, Morocco and Iringa Airport, Tanzania for 1 - 6 November and 27 February- 4 March 2023 respectively. GFS forecasts (blue lines) and observations (black dots). Weather station locations are shown in map inset at right.

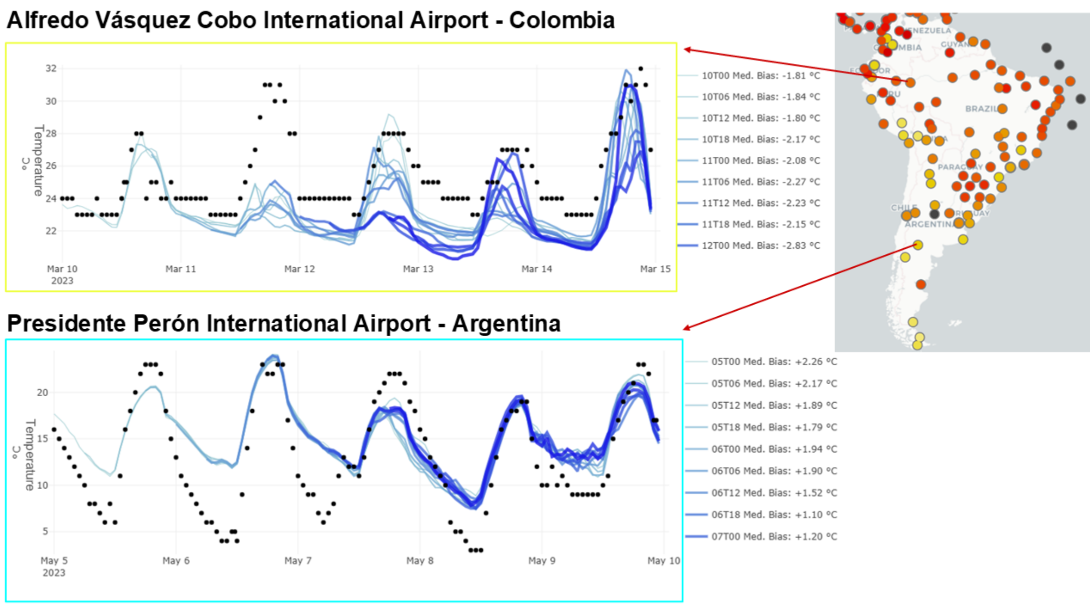

Figure 1.2: Time series of GFS temperature forecasts at Alfredo Vásquez Cobo International Airport - Colombia and Presidente Perón International Airport - Argentina for 10-15 March and 5 - 10 May, 2023 respectively. GFS forecasts (blue lines) and observations (black dots). Weather station locations are shown in map inset at right.

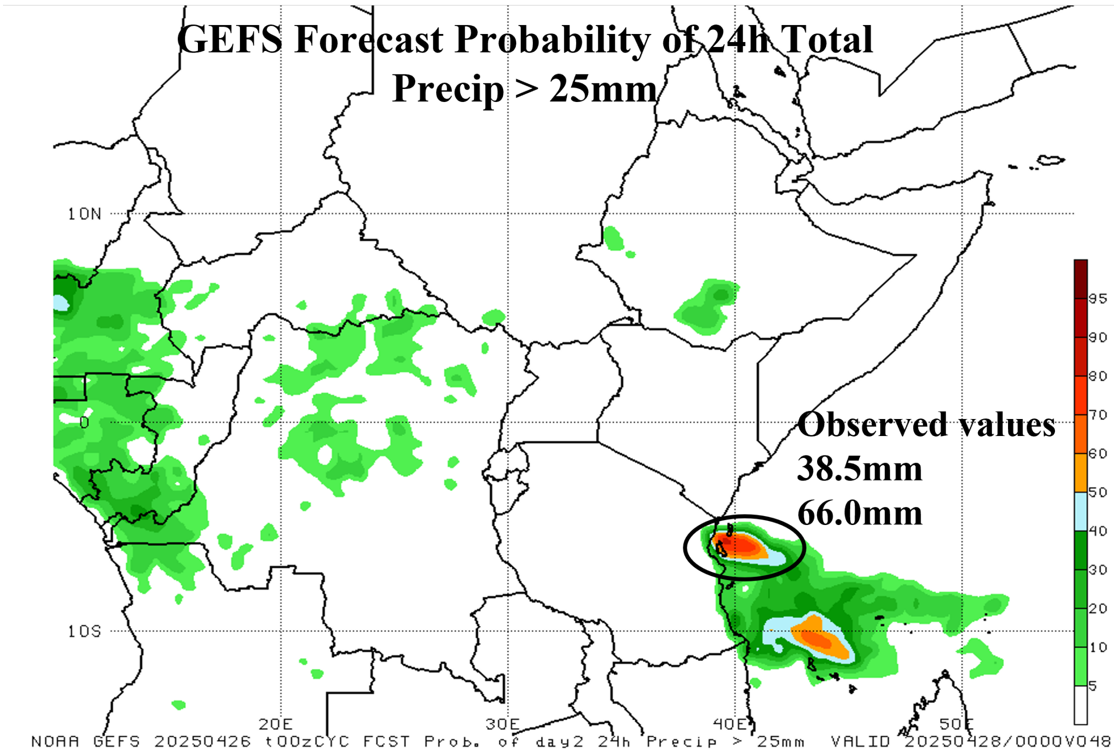

Figure 1.3: GEFS probabilistic forecast for East Africa for 28 April 2025 at 0 UTC showing precipitation likelihood of >25 mm in 24 hours and the amount of precipitation which was recorded on the day of the event.

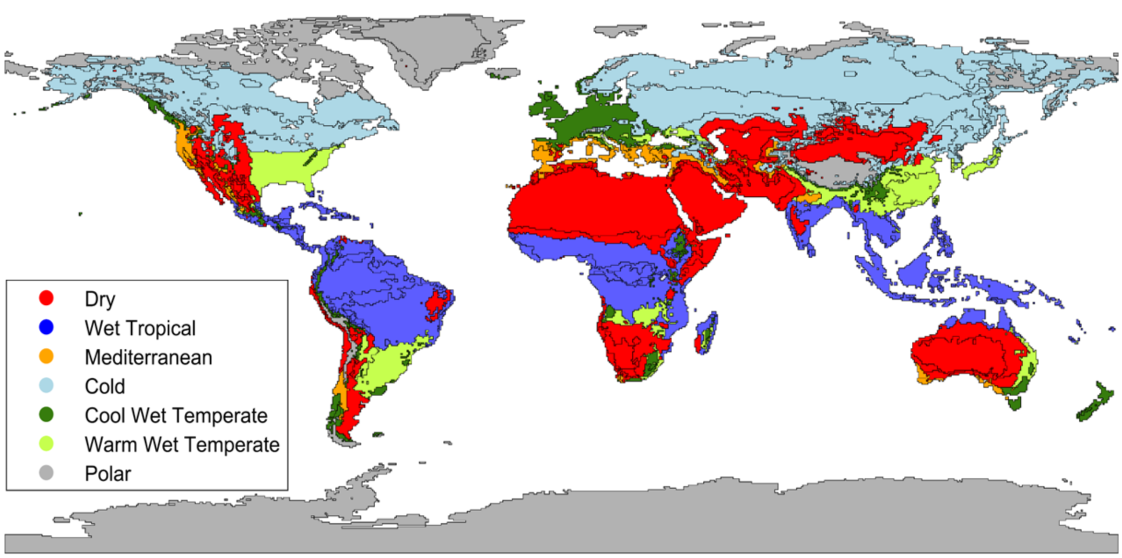

Figure 1.4: World map showing the seven simplified climate zones used in this study based on Köppen-Geiger climate classification (Kottek et al. 2006).

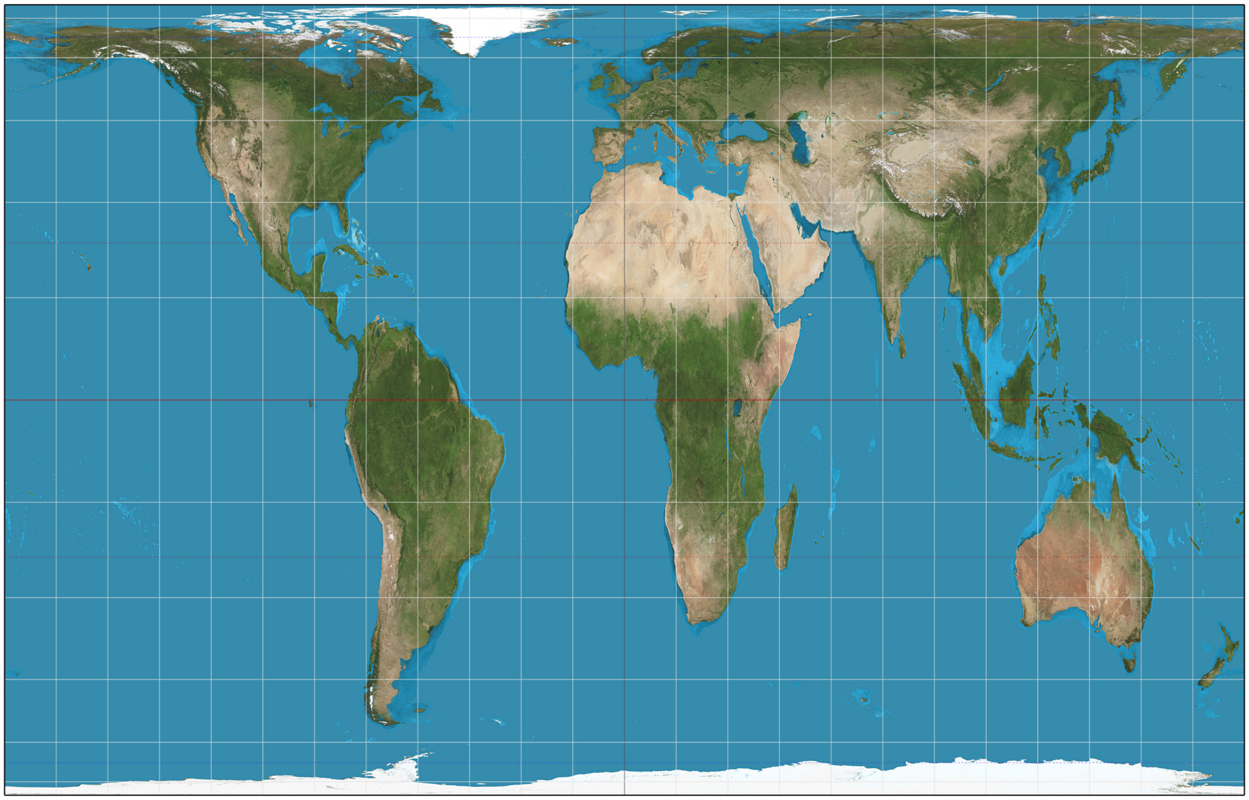

Figure 1.5: Land cover world map shown with the Gall-Peters projection, a cylindrical equal area map projection, that facilitates comparisons of the relative sizes of land areas. Source: en.wikipedia.org/wiki/File:Gall–Peters_projection_SW.jpg

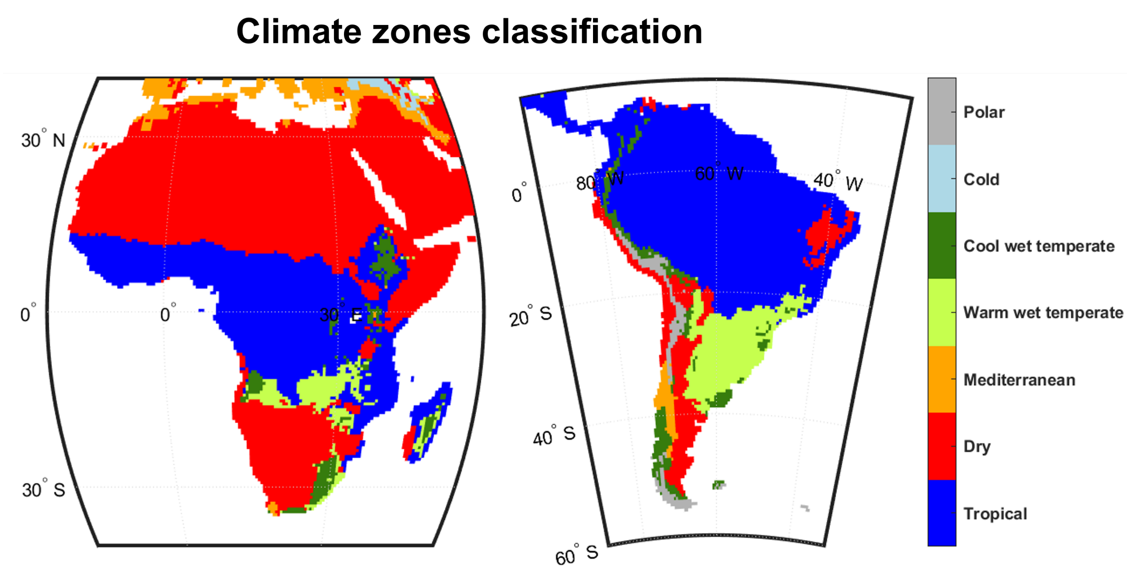

Figure 1.6: Simplified climate zones for Africa and South America based on Koppen-Geiger classification. Tropical (blue), Dry (red), Mediterranean (orange), Warm Wet Temperate (green), Cool Wet Temperate (dark green), Cold (light blue), and Polar (gray).

Figure 1.7: Elevation Map of Africa.(https://www.gif-map.com/maps-of-africa/elevation-map-of-africa)

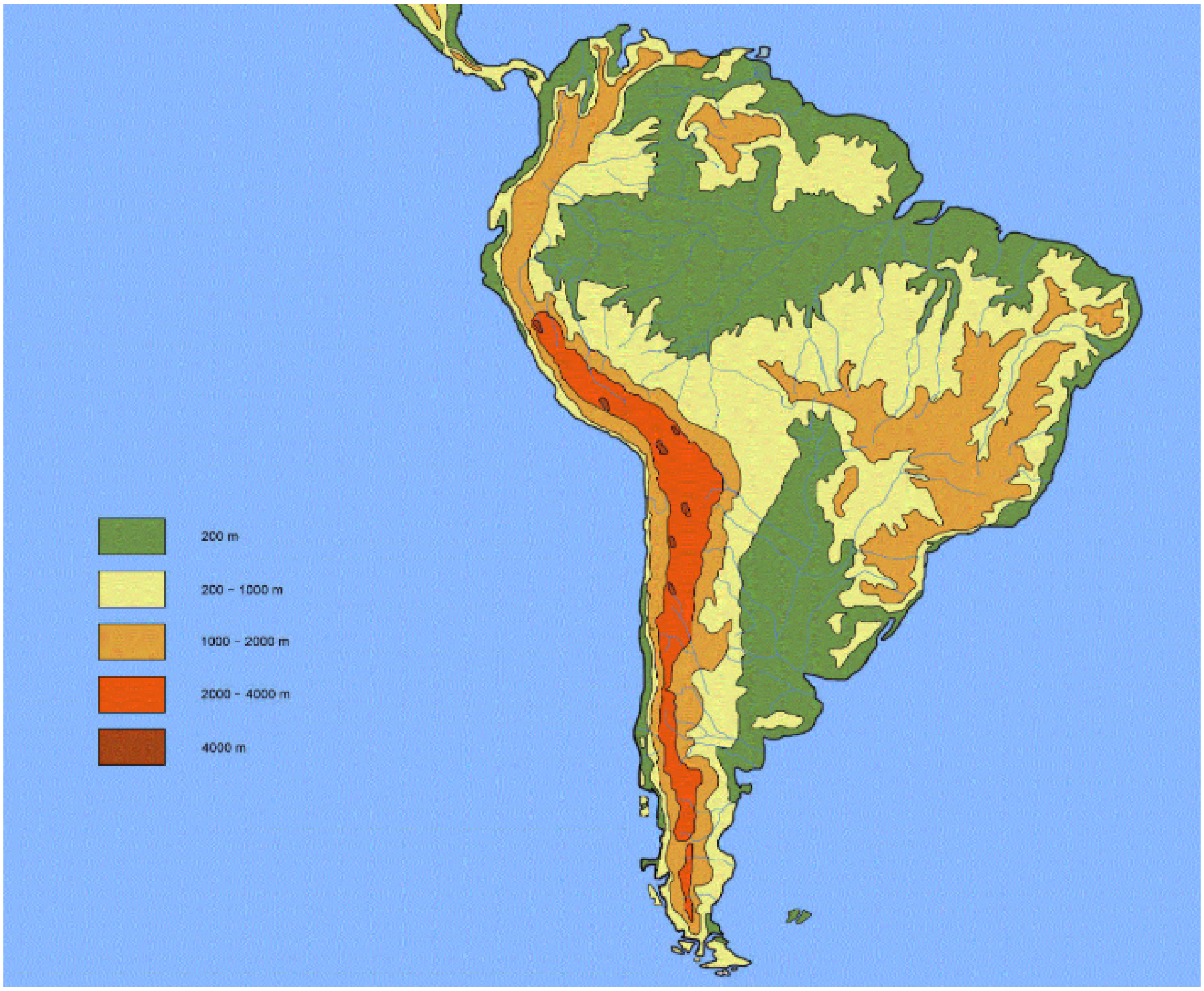

Figure 1.8: Elevation Map of South America.(www.gif-map.com/maps/south-america/elevation-map-of-south-america.gif)

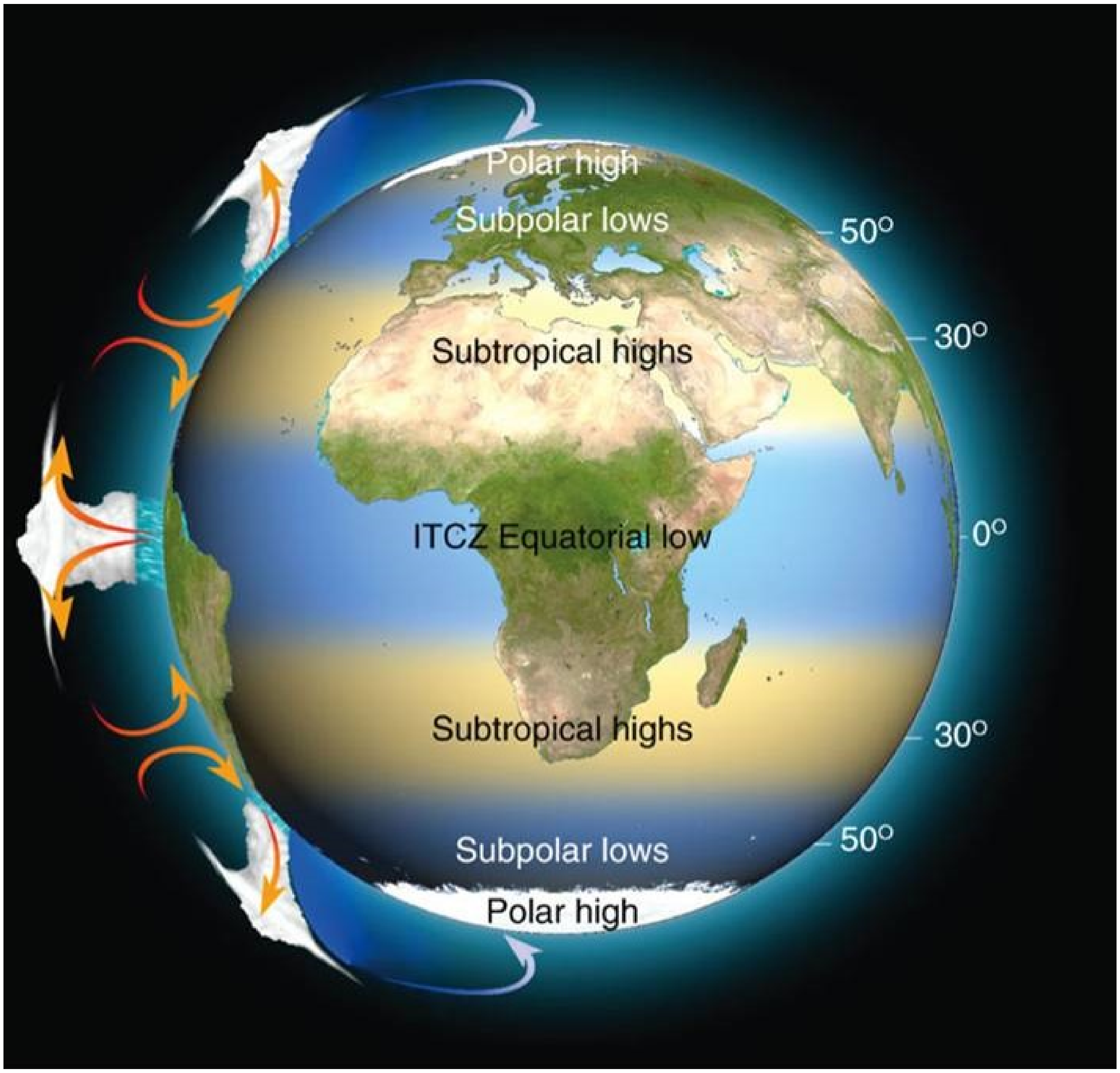

Figure 1.9: Idealized depiction of rising and sinking air within Earth's general circulation at the time of equinox when the sun is directly over the equator. The rising air of the ITCZ straddles the African continent with the sinking air yielding desert areas in north Africa and south Africa. Source: Ahrens and Henson (2018).

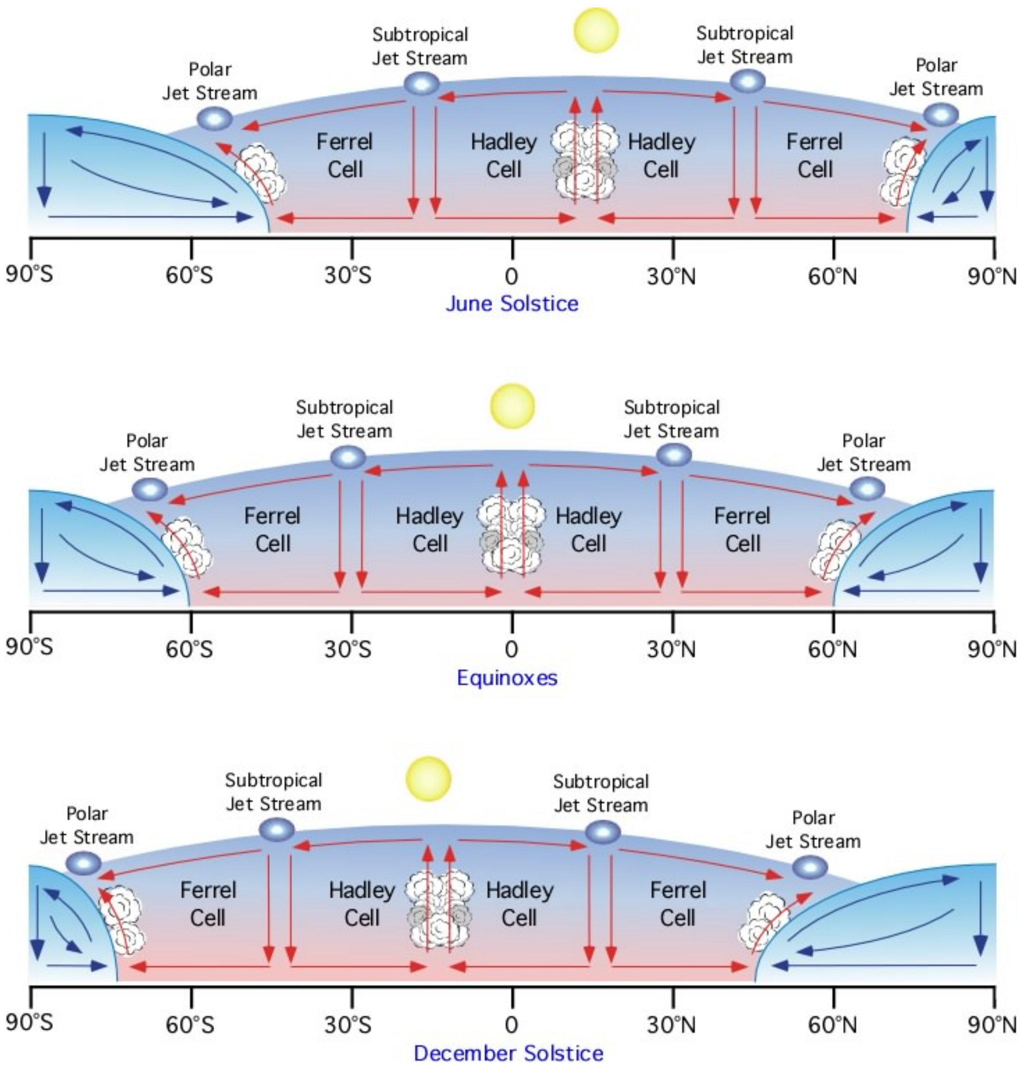

Figure 1.10: Seasonal shifts in the latitudes of different cells within the global circulation patterns. The ITCZ is between the two Hadley cells. (Source: http://www.physicalgeography.net/fundamentals/7u.html)

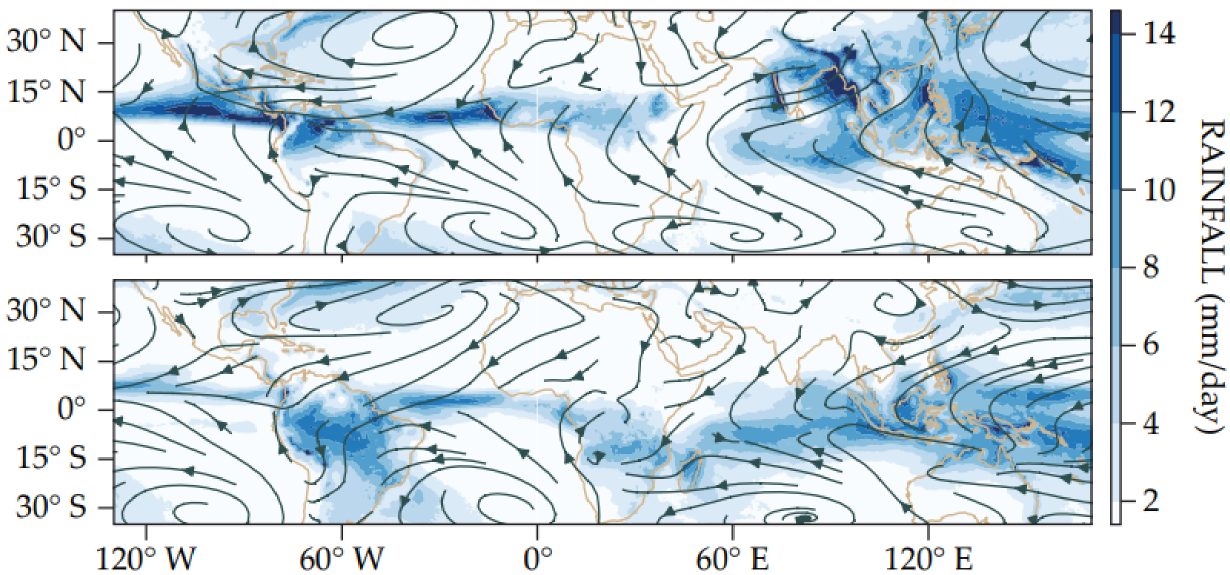

Figure 1.11:   Tropical rainfall (blue shading) and converging near-surface wind patterns that occur in the Northern Hemisphere (June–September, top) and the Southern Hemisphere (December–March, bottom), adapted from Biasutti et al. (2023)

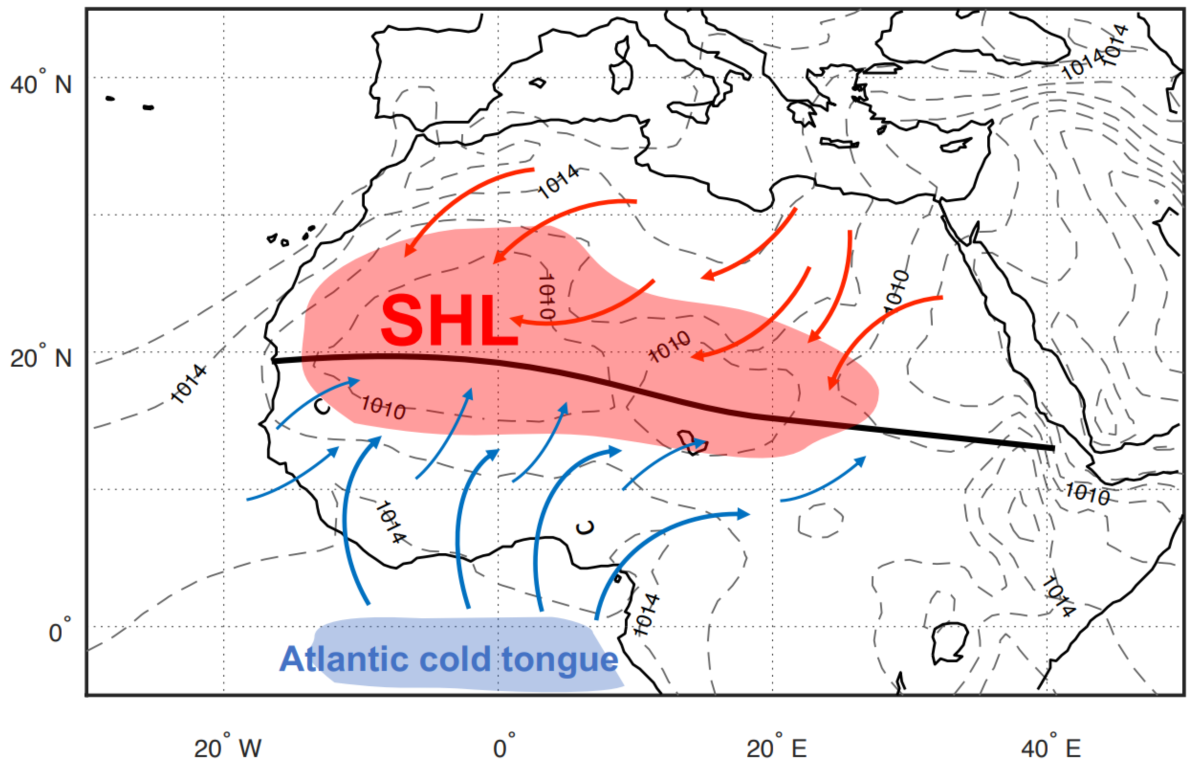

Figure 1.12: Schematic of West African Monsoon based on July-September long term average surface pressure and surface winds. Blue arrows indicate winds bringing moisture from Atlantic Ocean and red arrows indicate dry winds from the Sahara Heat Low (SHL) region. The winds converge at the ITCZ (black line). From Berntell (2023).

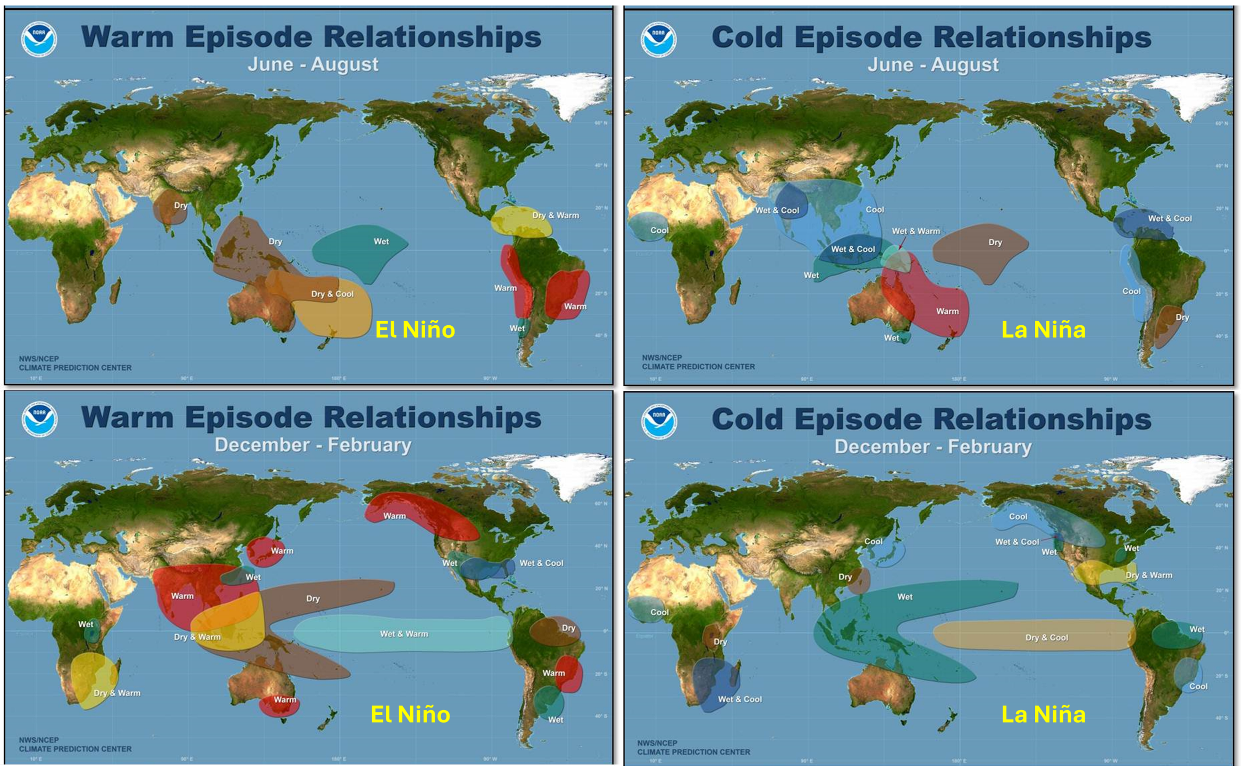

Figure 1.13: Typical temperature and precipitation impacts of a strong El Nino (ENSO warm phase) and strong La Nina (ENSO cold phase) compared to neutral conditions for JJA and DJF. (Source: NOAA/NCEP Climate Prediction Center.)

CHAPTER

2

DATA AND METHODS

2.1 Data

We examine the diurnal variation of temperature and dew point forecast biases, by comparing hourly predictions to observed values for 7 am local time (representing near daily minimum temperature) and 3 pm local time (representing near daily maximum temperature) (e.g. Fig. 2.1). The study period is from December 2021 to November 2024, which comprises 3 years of four seasons (DJF, MAM, JJA, SON) for both Africa and South America. The accuracy of predictions from the GFS model are assessed across multiple weather stations in Africa and South America. By evaluating forecast biases and performance, the study highlights the strengths and weaknesses of GFS under different climate and geographical conditions.

Key terms relevant to this study include: *initialization time*, which is the starting point of a model run; *lead time*, the interval between the initialization of a forecast and the time it predicts: and *valid time*, the specific time that a forecast is intended to describe. This analysis focuses on approximately 48-hour lead times and compares matched weather station observations with model forecasts.

2.1.1 Global Forecast System (GFS) Model

The GFS model is run by NOAA's National Centers of Environmental Prediction (NCEP) Environmental Modeling Center (EMC). The GFS operates with a 13 km resolution grid internally, while its output is distributed on a 0.25 degree grid, equating to a spatial resolution of approximately 27-28 km. Forecasts are generated every six hours at 0000, 0600, 1200, and 1800 UTC. We use data from GFS version 16 (GFSv16), which was introduced in March 2021 (Yang and Treadon 2020) and was the operational version running as of December 2024. Details on GFS parameterizations are given in Appendix Table 5.1.

GFS model data are obtained through NOAA's database on the AWS cloud service. As part of the standard variables output by GFS in the grid files they distribute are air temperature, dew point and Relative Humidity (RH) at 2-m above ground level. This GFS 2-m product is produced expressly for the purpose of comparing to observations. Prior to distribution, the GFS output undergoes processing by the Unified Post Processor (UPP), a tool used across NOAA's operational models to convert their raw model output into standardized pressure levels and grids. For the purposes of this analysis, we spatially interpret the 0.25 degree grid values using linear interpolation methods to match the precise station coordinates (Patel et al. 2021).

Since GFS model forecasts are initialized every 6 hours at 00 UTC, 06 UTC, 12 UTC and 18 UTC, the 48-hour lead time does not always align perfectly with the 7 AM or 3 PM local time at all locations. To address this, we use a *lead-time ish* method that selects the nearest available forecast hour within a specific window but not after the target time. For example, for a station at longitude of 30°E in central Africa, the UTC time corresponding to the daily minimum temperature at 7 am local time is 5 UTC. To obtain the 48hourish forecast for 5 UTC on 10 Jan 2024, we would use the 47-hour lead time forecast which was initialized at 6 UTC on 8 Jan 2024.

2.1.2 Surface Weather Observations

Numerical weather model forecasts are evaluated against hourly surface observations from Meteorological Terminal Air Reports (METAR) and Automated Surface Observing Systems (ASOS) at airports. METAR data are filtered to retain only one observation per hour for each variable. In cases where temperature data are missing, values are interpolated using the nearest available observation. However, if gaps exceed six hours, they are marked as missing (NaN).

Some stations in Africa and South America routinely report hourly values during daylight hours but have data gaps overnight. Fortunately, the available values usually include observations taken at 7 AM and 3 PM local time. To be included in the analysis, a station must have valid temperature observations for at least 70 percent of the total 7 AM and 3 PM hours. After these quality checks, there are 105 weather stations in Africa and 98 stations in South America (Fig. 2.2). Most of these locations are along the coasts where population density is higher than within the interiors of each continent. Most METAR hourly reports from outside the US do not include precipitation data. We address precipitation context indirectly using satellite data (Sections 2.3.1 and 2.3.2).

2.1.3 Definition of Model Biases

Model biases were quantified by comparing forecasted values to observed values at the same valid time. The model bias is defined as:

$$\text{Model Bias} = \text{Forecast Value} - \text{Observed Value} \tag{2.1}$$

For air temperatures, a positive bias indicates that the model predicts warmer temperatures than observed, while a negative bias indicates colder predictions. For dew points, a positive bias indicates that the model predicts wetter water vapor contents than observed, while a negative bias indicates dryer predictions.

Model biases were computed for 7 am and 3 pm local time for each day and each station in Africa and South America during the 3 year study period. These hourly bias values are compiled into various seasonal and annual statistics and are discussed in Chapter 3.

2.2 Definitions of Seasons

In addition to examining overall annual forecast biases by climate zone, we also wanted to group the bias statistics into physically meaningful subsets by defining similar seasonal conditions between the two continents. Our initial idea was to do this in terms of "wet" and "dry" seasons. However, although both continents are influenced by the seasonal variations of the Intertropical Convergence Zone (ITCZ) (Hagos and Cook 2005), additional factors such as topography, oceanic influences, and land surface processes contribute to different timing of "wet" and "dry" seasons between Africa and South America. Given these differences, we adopted the conventional 3-month seasons: December-January-February (DJF), March-April-May (MAM), June-July-August (JJA), and September-October-November (SON). These seasonal divisions generally capture the dominant precipitation patterns, though with some key regional variations. For instance, while JJA is largely a dry season in much of Africa, the northern part of South America experiences peak rainfall during this period (Fig. 2.3).

2.3 Seasonal Variations

2.3.1 Precipitation Context

Precipitation patterns vary significantly by region, influenced by factors such as topography, vegetation cover, proximity to large water bodies, and seasonal changes. Along with land cover type, precipitation is a primary control on soil moisture that modulates both air temperature and dew point. In this study, we do not analyze hourly precipitation data but instead define precipitation regimes to identify wet and dry seasons. These regimes will be used to interpret and analyze biases in temperature and dew point. Hourly precipitation data are not available from the weather station data set in Africa and South America, so we cannot assess variations in temperature and dewpoint in the context of individual storms. Instead, we examined average precipitation on monthly and seasonal time scales.

The Global Precipitation Climatology Project (GPCP) monthly dataset provides precipitation estimates on a 2.5 by 2.5 degrees grid from 1979 to the present. GPCP combines satellite-based microwave and infrared retrievals with rain gauge observations over land, offering a reliable long-term record of precipitation. This dataset is widely used to analyze precipitation trends and assess seasonal variability.

Figure 2.3 illustrates the average seasonal precipitation for each of the twelve 3-month seasons used in this analysis. Each row represents a different season. Each column represents a different year for a given season. The spatial patterns of precipitation are broadly consistent for a given season year to year. The Amazon basin receives substantial rainfall in DJF, MAM, and JJA. The northern portions of the basin see monthly average values > 10 mm/day from March-August. The driest portions of South America are along the subtropical portions of the Chilean coast. Over March-August, the rain forest in central Africa has smaller average rain rates compared to the Amazon, with typical values between 5-7 mm/day. Tropical eastern Africa has moderate rainfall averaging 3-6 mm/day from December - March and is dryer the other half of the year. The latitude range of Africa 35°N to 30°S to includes two subtropical desert areas in the Sahara and southern Africa.

2.3.2 Vegetation Context

The Normalized Difference Vegetation Index (NDVI) is a satellite-derived metric that quantifies vegetation density by measuring the "greenness" of Earth's surface. It is widely used to track seasonal and long-term vegetation changes, helping scientists analyze how land cover responds to climatic and environmental conditions, (Huete et al. 2002). In this study, NDVI data were used solely to provide seasonal context.

NDVI is calculated using reflectance values from red and near-infrared wavelengths, taking advantage of the fact that healthy plants absorb red light for photosynthesis while reflecting near-infrared light (Rouse et al. 1974). By combining these spectral bands, NDVI provides a reliable indicator of vegetation growth and stress. Data for NDVI come from NASA's Moderate Resolution Imaging Spectroradiometer (MODIS) aboard the Terra satellite, which offers global-scale measurements that allow for spatial and temporal comparisons of vegetation trends. These data are used in a range of applications, from monitoring agricultural productivity to detecting environmental changes.

The spatial distributions of vegetation through the year complement information on rainfall from GPCP (Section 2.3.1). While the tropical rain forests of the Amazon and Central Africa remain green throughout the year, the savannah areas of mixed grassland with a sparse trees vary seasonally. Increased vegetation in the savannah follows increased precipitation and vice versa.

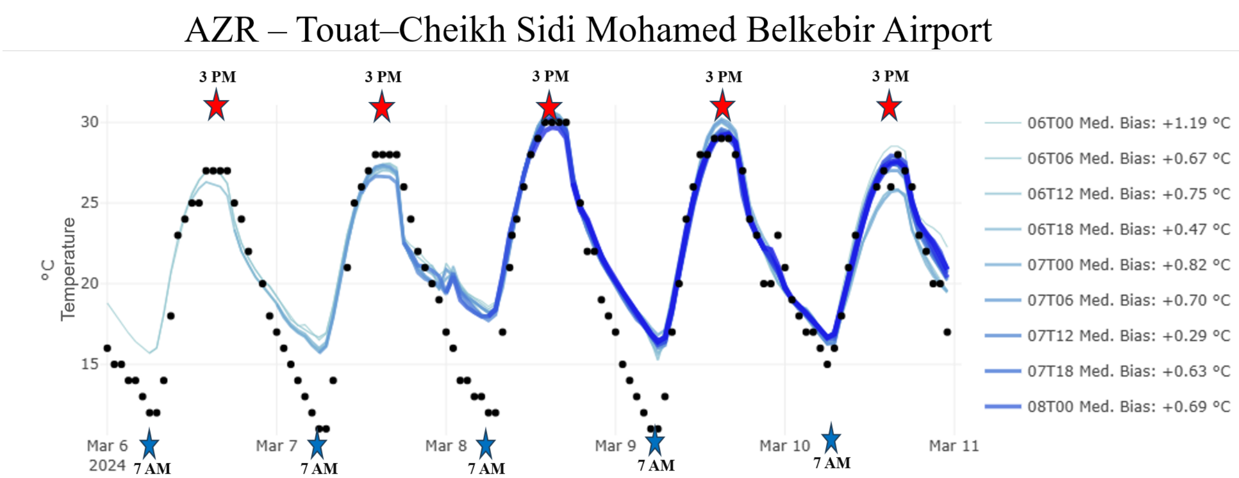

Figure 2.1: Example of GFS temperature forecasts for several initialization times (set of blue lines) and actual temperature observations (black dots) for Touat-Cheikh Sidi Mohamed Belkebir airport in Algeria from 6-11 March 2024. Highlighted stars indicate the timing for 7 AM and 3 PM local times

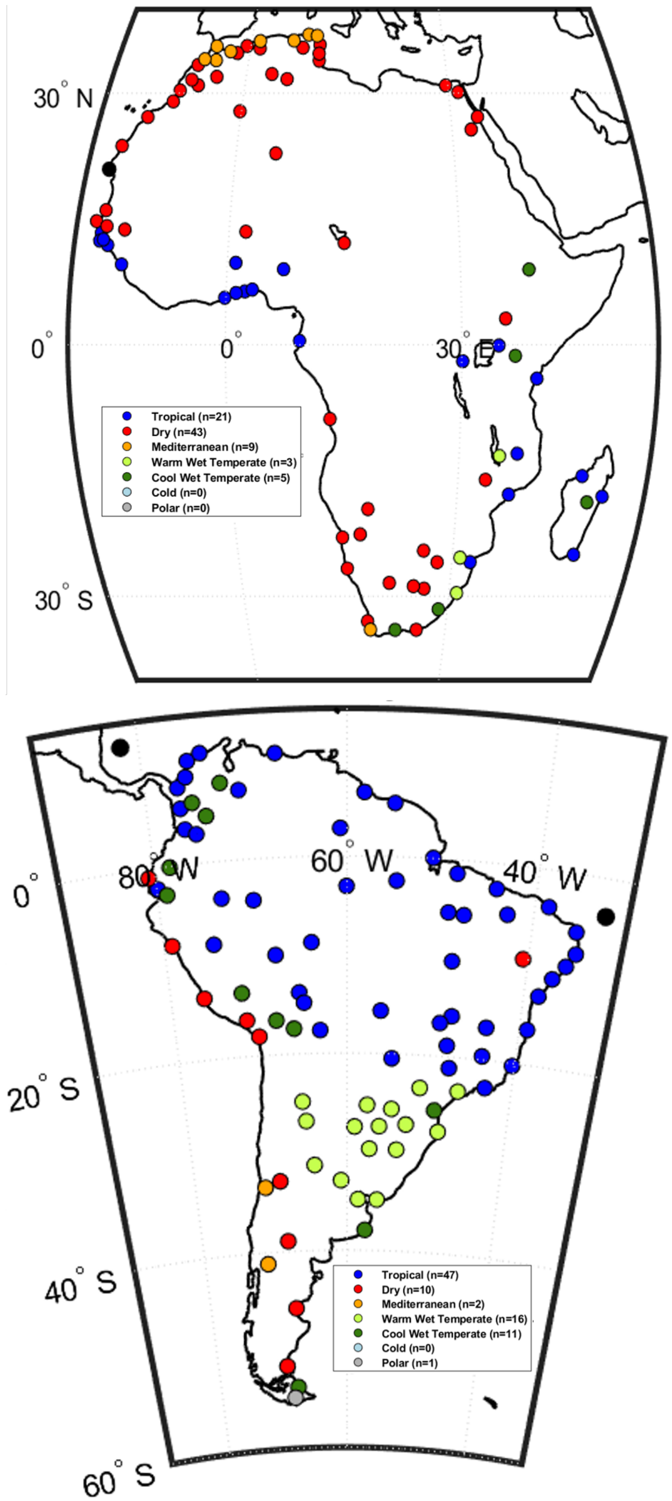

Figure 2.2: Map of Africa (top) and South America (bottom) weather stations color-coded by simplified climate zone classification. Each station is represented by a dot whose color corresponds to its climate zone—Tropical (blue), Dry (red), Mediterranean (orange), Warm Wet Temperate (green), Cool Wet Temperate (dark green), Cold (light blue), and Polar (gray). The number of stations in each climate zone indicated in legend.

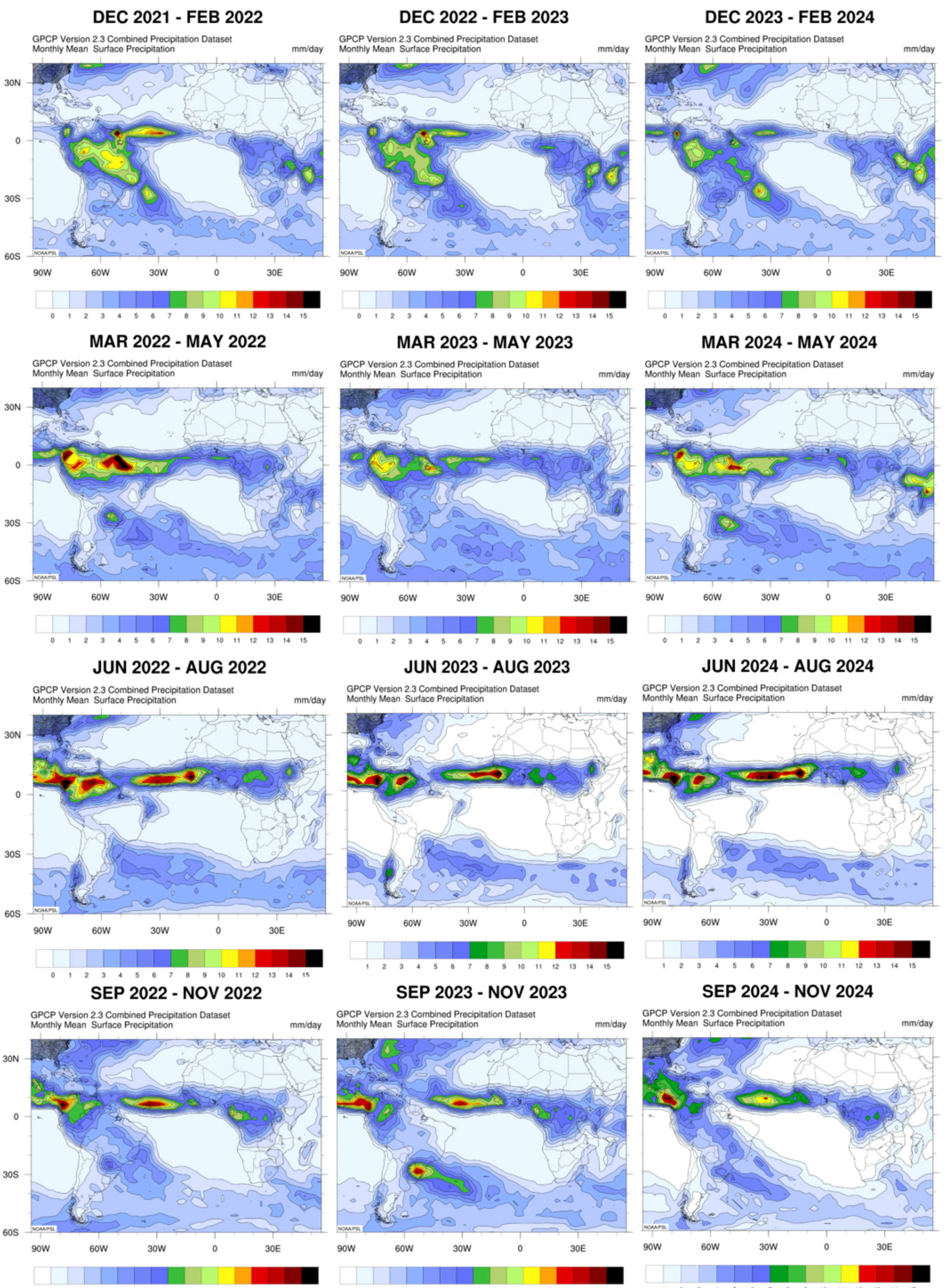

Figure 2.3: GPCP maps showing average seasonal precipitation (mm/day) received in South America and Africa from 2022 to 2024.

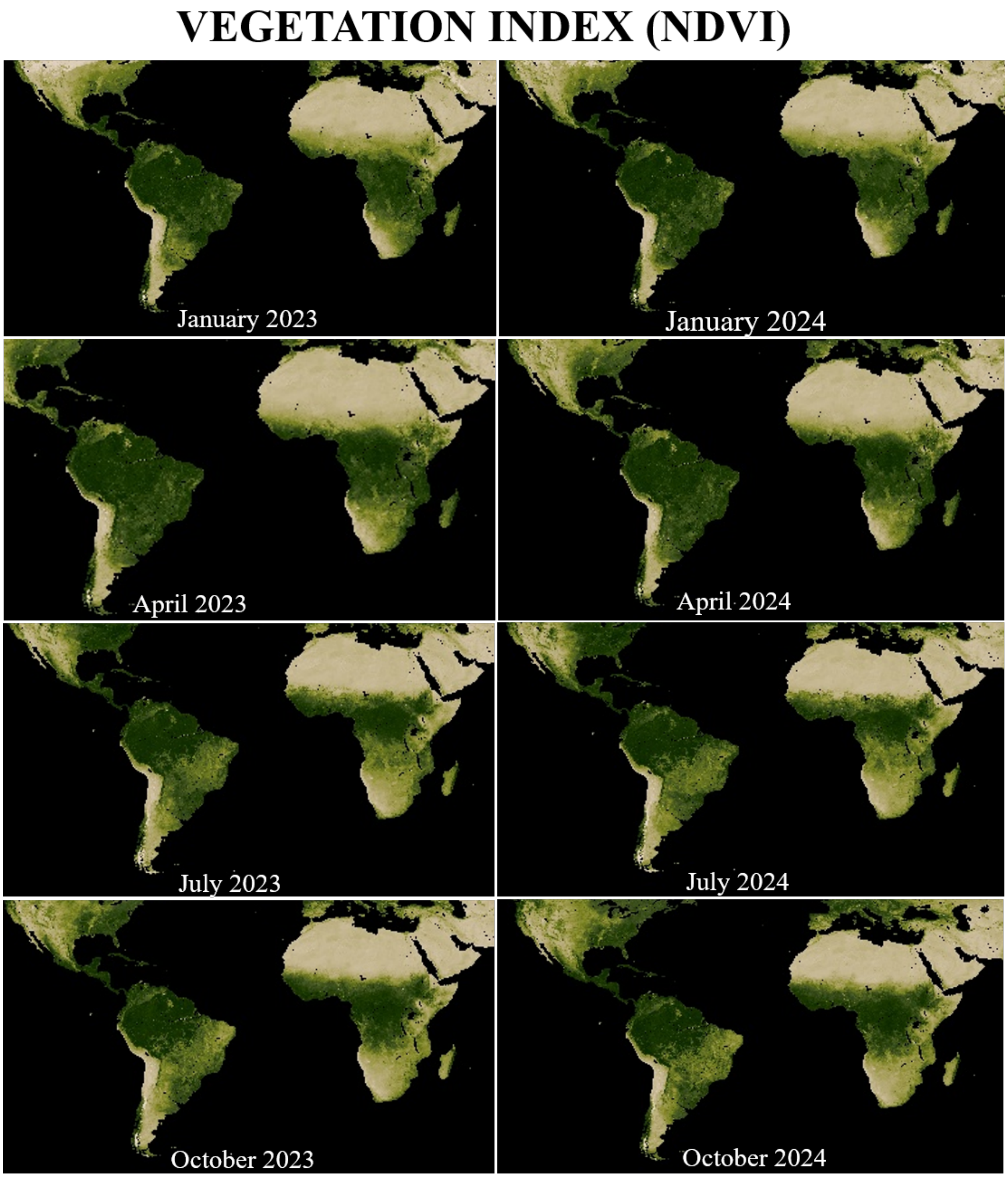

Figure 2.4: NDVI maps, with one representative month per season (January, April, July, and October), derived from NASA's MODIS satellite data, illustrating vegetation density and seasonal variations in South America and Africa over two years.

CHAPTER

3

RESULTS- ASSESSMENT OF TEMPERATURE AND DEWPOINT BIASES IN GFS ACROSS AFRICA AND SOUTH AMERICA

We examined the 48hourish GFS forecast biases in temperature and dewpoint for each station and each 7 am and 3 pm local time over 3 years comprising over 200,000 matched model to observation comparisons. Statistics are compiled in terms of the characteristics of annual distributions as well seasonal distributions.

3.1 Annual biases across the climate zones

The distributions combining data for all 3 years of 7 AM and of 3 PM biases for air temperature and for dewpoint are shown in Figure 3.1 by climate zone. Year to year, there is consistency in temperature bias and dewpoint bias distributions for a given climate zone among the three years (Appendix, Figs. 5.1, 5.2, 5.3). Key statistics of these distributions year by year are summarized in Tables 3.1, 3.2, 3.3 and 3.4. Average bias statistics for the 3 years are tabulated in Appendix Tables 5.2, 5.3, 5.4 and 5.5.

We will consider that median biases $< \pm 1°C$ *and 10th or 90th percentile biases* $< \pm 5°C$ *are* *within a reasonable margin of error and focus the discussion below on the "problem" climate zones and times that are outside of these thresholds.*

3.1.1 Annual Statistics for Air Temperature

Table 3.1: Summary statistics by climate zone for Africa air temperature bias distributions from Appendix Figs. 5.1, 5.2, 5.3 including the 10th, 25th, 50th, and 90th percentiles. Under each column for a percentile the yearly values for 2022, 2023 and 2024 are listed separately. Averaged values are in Table 5.2. Highlighted in color are values with a median biases > ±1°C.

Climate Zone	10th	25th	**50th (Median)**	75th	90th
Tropical 7am	–2.4 | -2.4 | -2.4	-1.3 | -1.3 | -1.3	**-0.2 | -0.3 | -0.4**	0.8 | 0.8 | 0.7	1.9 | 2.0 | 2.0
Tropical 3pm	-3.9 | -4.1 | -4.0	-2.6 | -2.7 | -2.6	**-1.3 | -1.3 |-1.3**	0.2 | 0.3 | 0.2	2.1 | 2.1 | 2.1
Dry 7am	-1.6 | -1.9 | -1.8	-0.5 | -0.8 | -0.7	**0.8 | 0.5 | 0.6**	2.6 | 2.3 | 2.4	4.5 | 4.4 | 4.2
Dry 3pm	-3.2 | -3.3 | -3.2	-1.9 | -2.0 |-1.9	**-0.6 | -0.8 | -0.7**	0.6 | 0.4 | 0.5	2.1 | 1.9 | 2.0
Mediterranean 7am	-1.9 | -2.0 | -2.0	0.7 | -0.8 | -0.9	**0.7 | 0.7 | 0.6**	2.6 | 2.5 | 2.3	4.5 | 4.3 | 4.1
Mediterranean 3pm	-2.6 | -2.8 | -2.6	-1.7 | -1.8 | -1.8	**-0.8 | -0.9 | -0.8**	0.3 | 0.1 | 0.2	1.4 | 1.2 | 1.5
Warm Wet Temperate 7am	-1.7 | -2.0 | -2.4	-0.7 | -1.1 | -1.1	**0.1 | 0.1 | 0.1**	1.1 | 1.0 | 0.9	2.7 | 2.2 | 2.1
Warm Wet Temperate 3pm	-1.9 | -2.5 | -2.0	-0.9 | -1.2 | -1.0	**0.4 | 0.4 | 0.3**	2.1 | 2.3 | 2.2	3.9 | 4.0 | 3.8
Cool Wet Temperate 7am	-2.7 | -2.7 | -2.6	-1.8 | -1.7 | -1.7	**-0.8 | -0.8 | -0.7**	0.3 | 0.4 | 0.5	1.9 | 1.7 | 2.2
Cool Wet Temperate 3pm	-3.9 | -4.0 | -4.0	-2.3 | -2.6 | -.26	**-1.0 | -1.2 | -1.3**	0.3 | 0.0 | 0.0	1.7 | 1.3 | 1.3

Table 3.2: Summary statistics by climate zone for South America air temperature bias distributions from Appendix Figs. 5.1, 5.2, 5.3 including the 10th, 25th, 50th, and 90th percentiles. Under column for a percentile the years values for 2022, 2023 and 2024 are listed separately. Highlighted in color are values with a median biases > ±1°C and 10th or 90th percentile biases > ±5°C.

Climate Zone	10th	25th	**50th (Median)**	75th	90th
Tropical 7am	-2.6 | -2.6 | -2.6	-1.7 | -1.7 | -1.7	**-0.8 | -0.7 | -0.7**	0.2 | 0.4 | 0.4	1.4 | 1.6 | 1.6
Tropical 3pm	-4.6 | -4.4 | -4.4	-2.7 | -2.5 | -2.3	**-0.9 | -0.6 | -0.5**	1.1 | 1.5 | 1.7	3.0 | 3.7 | 3.8
Dry 7am	-2.5 | -2.7 | -2.5	-1.4 | -1.7 | -1.5	**-0.2 | -0.7 | -0.5**	1.1 | 0.5 | 0.6	3.0 | 2.5 | 2.4
Dry 3pm	-3.8 | -3.8 | -3.9	-2.4 | -2.5 | -2.4	**-0.9 | -1.2 | -0.9**	0.5 | 0.1 | 0.4	1.7 | 1.3 | 1.4
Mediterranean 7am	-4.4 | -4.2 | -4.3	-2.2 | -2.3 | 1.0	**1.0 | 0.7 | 1.0**	3.7 | 3.1 | 3.5	**6.4 | 5.6 | 5.0**
Mediterranean 3pm	-4.6 | -4.4 | -4.4	-2.9 | -2.7 | -3.0	**-0.7 | -1.6 | -1.1**	0.9 | 0.4 | 0.6	2.5 | 1.7 | 1.9
Warm Wet Temperate 7am	-2.2 | -2.5 | -2.6	-1.2 | -1.4 | -1.6	**0.0 | -0.2 | -0.4**	1.5 | 1.3 | 0.9	3.2 | 2.8 | 2.6
Warm Wet Temperate 3pm	-2.8 | -3.1 | -3.0	-1.5 | -1.6 | -1.5	**0.0 | 0.0 | 0.1**	1.8 | 2.1 | 1.9	3.6 | 4.2 | 4.1
Cool Wet Temperate 7am	-3.7 | -3.9 | -3.9	-2.5 | -2.5 | -2.6	**-1.0 | -1.0 | -1.1**	0.4 | 0.3 | 0.2	2.0 | 1.9 | 1.5
Cool Wet Temperate 3pm	**-7.6 | -7.9 | -8.2**	-5.6 | -5.7 | -6.1	**-2.9 | -2.8 | -3.0**	-0.7 | -0.8 | -0.8	0.8 | 0.9 | 0.8

Air temperature bias distribution statistics by climate zones in Africa (Table 3.1) and in

South American (Table 3.2) show that median biases are mostly less than ±1°C. Tropical and Cool Wet Temperate climate zones have slightly larger magnitude negative biases in Africa and South American as compared to the other climate zones.

For the Cool Wet Temperature zone, temperature median biases are cooler in South America (3 pm median biases for each year of -2.9, -2.8 and -3.0°C) as compared to Africa (median biases for each year of -1.0, -1.2 and -1.3°C). African Tropical zones have a -1.3°C temperature bias in the afternoon, whereas South American Tropical zone biases stay under -1°C.

In South America, the Mediterranean at 7 am zone stands out with a median bias of 1°C, indicating a warm bias, while the Mediterranean at 3 pm shows a cold bias of -1.1°C. The afternoon temperatures often have a small cool bias in multiple climate zones on both continents. One possible reason is that the model may be overestimating cloud cover in the afternoon, which would reflect sunlight and reduce the amount of solar energy reaching the ground.

When looking at the 10th and 90th percentiles (see the tails of the violin distributions in Figure 3.1abcd), only South America shows biases > ±5°C. The Cool Wet Temperate zone at 3 pm has a long tail with a 10th percentile bias of -7.9°C while the Mediteranean zone at 7 am has a 90th percentile bias of 5.7°C. These outliers clearly indicate that GFS model is significantly struggling in these regions. In contrast, there were no pronounced long tails in Africa for the same climate zones.

3.1.2 Annual Statistics for Dew Point Temperature

Table 3.3: Summary statistics by climate zone for Africa dew point bias distributions from Appendix, Figs. 5.1, 5.2 and 5.3 including the 10th, 25th, 50th, and 90th percentiles. Under column for a percentile the years values for 2022, 2023 and 2024 are listed separately. Highlighted in color are values with a median biases > ±1°C and 10th or 90th percentile biases > ±5°C.

Climate Zone	10th	25th	**50th (Median)**	75th	90th
Tropical 7am	-3.4 | -4.0 | -4.3	-2.5 | -2.5 | -2.6	**-1.6 | -1.6 | -1.7**	-0.7 | -0.8 | -0.9	0.2 | 0.1 | 0.1
Tropical 3pm	-4.7 | -5.0 | -5.2	-3.0 | -3.1 | -3.2	**-1.2 | -2.0 | -2.0**	-0.8 | -0.9 | -0.9	0.6 | 0.3 | 0.5
Dry 7am	-5.4 | -5.5 | -5.6	-3.2 | -3.2 | -3.3	**-1.4 | -1.5 | -1.6**	0.1 | 0.0 | 0.0	1.8 | 1.7 | 1.7
Dry 3pm	-6.4 | -6.6 | -6.9	-4.0 | -4.2 | -4.3	**-1.8 | -2.0 | -2.1**	0.1 | -0.1 | -0.1	2.2 | 2.0 | 2.0
Mediterranean 7am	-3.9 | -4.2 | -4.3	-2.4 | -2.5 | -2.8	**-1.0 | -1.1 | -1.4**	0.3 | 0.3 | -0.2	1.8 | 1.7 | 1.2
Mediterranean 3pm	-4.6 | -5.0 | -5.0	-3.0 | -3.1 | -3.3	**-1.4 | -1.6 | -1.8**	-0.1 | 0.0 | -0.4	1.7 | 1.6 | 1.2
Warm Wet Temperate 7am	-3.0 | -3.3 | -4.4	-1.8 | -2.0 | -2.7	**-0.8 | -1.1 | -1.1**	0.1 | -0.2 | -0.2	1.1 | 0.8 | 0.8
Warm Wet Temperate 3pm	-4.6 | -5.0 | -5.3	-2.7 | -3.0 | -3.4	**-1.1 | -1.2 | -1.6**	0.0 | 0.2 | -0.1	1.0 | 1.3 | 1.4
Cool Wet Temperate 7am	-3.8 | -3.7 | -3.9	-2.6 | -2.7 | -2.7	**-1.7 | -1.8 | -1.7**	-0.8 | -0.8 | -0.8	0.2 | 0.1 | 0.4
Cool Wet Temperate 3pm	-4.7 | -4.2 | -4.4	-3.0 | -2.8 | -2.7	**-1.6 | -1.5 | -1.3**	-0.3 | -0.3 | 0.0	0.8 | 0.8 | 1.2

Table 3.4: Summary statistics by climate zone for South America dew point bias distributions from Appendix, Figs. 5.1, 5.2, 5.3 including the 10th, 25th, 50th, and 90th percentiles. Under column for a percentile the years values for 2022, 2023 and 2024 are listed separately. Highlighted in color are values with a median biases > ±1°C and 10th or 90th percentile biases > ±5°C.

Climate Zone	10th	25th	**50th (Median)**	75th	90th
Tropical 7am	-3.9 | -4.2 | -4.4	-2.6 | -2.6 | -1.6	**-1.6 | -1.6 | -1.6**	-0.8 | -1.6 | -0.8	-0.1 | -0.8 | -0.1
Tropical 3pm	-4.7 | -5.5 | -5.5	-2.9 | -3.2 | -3.4	**-1.6 | -1.8 | -1.9**	-0.4 | -0.5 | -0.7	0.7 | 0.6 | 0.4
Dry 7am	-4.5 | -4.0 | -3.8	-2.6 | -2.3 | -2.2	**-1.0 | -1.1 | -1.0**	0.4 | 0.2 | 0.0	1.8 | 1.8 | 1.3
Dry 3pm	-5.9 | -5.1 | -5.1	-3.4 | -3.1 | -3.3	**-1.9 | -1.8 | -1.5**	-0.1 | -0.5 | -0.3	1.5 | 1.2 | 1.1
Mediterranean 7am	-4.6 | -4.4 | -4.7	-3.0 | -3.1 | -3.1	**-1.6 | -1.6 | -1.7**	-0.1 | -0.3 | 0.0	1.6 | 1.0 | 1.5
Mediterranean 3pm	-5.2 | -5.1 | -5.2	-3.7 | -3.5 | -3.3	**-1.9 | -1.7 | -1.2**	0.1 | 0.1 | 0.4	2.0 | 1.7 | 2.5
Warm Wet Temperate 7am	-4.3 | -4.4 | -4.6	-2.7 | -3.0 | -3.1	**-1.4 | -1.8 | -1.7**	-0.1 | -0.4 | -0.5	1.2 | 0.9 | 0.7
Warm Wet Temperate 3pm	-5.5 | -5.9 | -5.8	-3.3 | -3.0 | -3.7	**-1.4 | -1.8 | -1.9**	0.1 | -0.2 | -0.4	1.7 | 1.3 | 1.1
Cool Wet Temperate 7am	-4.7 | -4.6 | -4.8	-3.4 | -3.2 | -3.4	**-1.7 | -1.6 | -1.8**	-0.3 | -0.1 | -0.4	1.2 | 1.3 | 1.0
Cool Wet Temperate 3pm	-3.7 | -3.6 | -3.6	-2.3 | -2.2 | -2.0	**-0.6 | -0.4 | -0.3**	1.1 | 1.3 | 1.5	3.0 | 3.0 | 3.1

GFS dewpoint temperatures are overall dry in nearly every climate zone in both the morning and afternoon.(Tables 3.3 and 3.4). Median biases in both continents across all climate zones had an average of lower than -1°C in the entire 3 year period. This highlights that GFS model has a consistent dry bias with an exception of only one climate zone in South America at 3 pm (Cool Wet Temperate zone).

Extreme values at the 10th percentile further indicate that GFS model is performing poorly in forecasting dew points. These long tails suggest that the model not only tends to be dry on average but also occasionally produces extremely dry forecasts especially during the afternoon (Fig. 3.1). For South America, 10th percentile values < -5°C occur in the afternoons for the Tropical, Dry, and Mediterranean climate zones.

There is no one simple explanation for the dry bias that works for both the higher vegetation Tropical zone and the low vegetation Dry and Mediterranean zones. Within GFS, soil moisture is initialized using NASA's Land Information System (LIS) and land cover uses the community NOAH Land Surface Model (LSM). Of the two, land cover varies on longer time scales than soil moisture and is less likely to be in error. There is a potential amplifying feedback in that if dew points are too low, then precipitation will be too low, and soil moisture will be too low. Further complicating matters, Hohenegger et al. (2009) found that the sign of the soil moisture-precipitation feedback varied with model grid scale with 25-km scale grids and parameterized convection having increasing precipitation with increasing soil moisture while 2.2 km grids with explicit convection have increasing precipitation with decreasing soil moisture. The differences were related to the sensitivity of precipitation development to the presence of stable vs. mixed layers between the surface and cloud base. In the 2.2 km grids, dry, warmer soils yield more vigorous thermals which in the net transport more moisture from the surface to the cloud level as compared to wetter, cooler soils.

3.2 Seasonal biases across the climate zones

Table 3.5: Wet and dry seasons in the subregions of Africa and South America. The southeastern subregion for South American refers to the highlands in the SE portion of Brazil.

SEASONS	AFRICA (Sub regions)		SOUTH AMERICA (Sub regions)	
Wet Season	DJF	East, Central and South	DJF	North, East, West and South
	MAM	East, West, Central and South	MAM	North, East, West and South
	JJA	West and Central	JJA	North and South
	SON	East, Central, South, West	SON	North, East, West and South
Dry Season	DJF	North and West	DJF	None
	MAM	North	MAM	None
	JJA	North , East and South	JJA	East and West
	SON	North	SON	Southeastern

To better understand both strengths and weaknesses of GFS model forecasts as well as the potential physical processes contributing to higher biases, we decompose the annual bias information by season.

3.2.1 Joint variability of air temperature and dew point biases

In this section, we explore if there is a clear association between dewpoint biases and temperature biases at the same station at the same local time season by season.

Across all four seasonal scatter plots for DJF, MAM, JJA, and SON from 2022 through 2024 (Figures 3.2, 3.3, 3.4 and 3.5) there is no strong covariant relationship between seasonal median air temperature and dew point biases at the same local time. The scatter plots show sets of points that lack a discernible linear relation between air temperature bias and dew point bias as indicated by the very low correlation coefficients (r^2 equals 0.033 at 7 am and 0.042 at 3 pm in DJF, 0.044 at 7 am and 0.000 at 3 pm in MAM, 0.000 at 7 am and 0.036 at 3 pm in JJA and 0.001 at 7 am.) The main finding based on the annual statistics of an overall dry dew point bias is evident in the season data in that the majority of stations are below the 0° dew point bias line for all four seasons.

An limited exception is for the Tropical climate zone during SON at 3 pm, which hints at a weak relationship between dryer dewpoint biases and increasing temperature bias greater than 2°C (Fig. 3.5) but the correlation coefficient for the regression line is only 0.164. SON is a wet season in much of tropical Africa and South America (Table 3.5). The GFS might be underestimating clouds in SON season, overestimating daytime heating and predicting a warmer afternoon temperature than observed. Higher daytime heating would be associated with more mixing of the boundary layer (stronger thermals) and lower near surface dew points.

While not a covariant relation between temperature and dewpoint, there is distinct pattern in the distribution of biases for DJF (and to a smaller degree in MAM and JJA) in that the warm temperature biases for 7 AM in the Dry climate zone tend to be larger than 3 PM (Fig. 3.2, 3.3, and 3.4). DJF is a wet season for most of South America and east, central and south Africa (Table 3.5). The GFS might be too cloudy in DJF, underestimating nocturnal radiative cooling, and predicting a warmer morning temperature than observed.

3.3 Geographic variability of air temperature and dew point biases by season

We analyzed the median air temperature and dewpoint biases at 7 am and 3 pm in Africa and South America for each three-month season. Spatial patterns of temperature biases varied by time of day, by climate zone, and seasonally.

3.3.1 Air Temperature

Median biases at each weather station for each season combining data for the three years are shown in Figures 3.6 and 3.7. For context, similar information but separated into each 3 month season for each year is presented in Appendix Figures 5.4 - 5.9.

December-January-February

For the season of DJF (Fig. 3.6abcd) across the 3-year period, patterns in temperature biases for the GFS 48-hour lead time under all cloud cover conditions revealed consistent negative biases across the tropical regions of both South America at both 7 am and 3 pm local times. The largest cold biases observed, over -6°C, were in the northern and eastern regions of South America in at 3 pm (Appendix, Figs. 5.4cd , 5.6cd and 5.8cd). Warm temperature biases were consistently observed over the southern regions of South America and over the dry regions of northern and southern Africa particularly at 7 am while maintaining neutral to small negative bias during the afternoon (less than -2°C).

March-April-May

For the period of MAM, across three years (Figs. 3.6efgh), the patterns shifted slightly compared to DJF, with South America showing a broader spatial distribution of negative biases from -2°C to -6°C at both 7 am and 3 pm from 10 deg N to 25 deg S latitude, indicating that GFS is underestimating temperatures during this season for the majority of the stations. On the other hand, a few stations with a Dry climate over the southern regions of the continent experienced positive biases which were ranging from 2°C to 4°C (Appendix, Figs. 5.6gh and 5.8gh).

Over the African continent during MAM, median temperature biases at 7 am were a mix of weak positive and negative values with most of the cold biases covering the tropical regions and neutral to slight warm biases covering most of the northern and southern Africa. At 3 pm, temperature biases were negative at the majority of the stations. A few exceptions over the central and southern Africa particularly in 2023 and 2024 had positive biases ranging from 2 °C to 4 °C (Appendix, Figs. 5.6ef and 5.8ef).

June-July-August

Moving to JJA season (Fig. 3.7abcd), the GFS 48-hour lead time temperature biases under all cloud cover conditions over a 3-year period revealed notable patterns across South America and Africa at 7 am and 3 pm local times. In South America at 3 pm, the model exhibited a consistent negative bias in the tropical regions as seen in the Appendix, Figs. 5.7d, particularly over the Amazon, with biases reaching as low as -6°C. At 7 am there was a slightly less pronounced negative biases, around -3°C, were observed over the Amazon. In other locations at 7 am there were near zero and slight positive biases of around 2°C for other climate zones as well as few tropical stations.

In Africa, the tropical regions displayed negative biases, though less intense compared to the ones in the tropical South America. Median bias values at individual stations in Africa typically ranged between -2°C and -4°C at both 7 am and 3 pm. Conversely, the drier regions of northern and southern Africa showed small positive biases at 7 am, often less than 4°C, transitioning to neutral or slightly negative biases by 3 pm. These patterns indicate the model's tendency to underestimate temperatures in humid, tropical areas while slightly overestimating them in dry regions during the morning hours of JJA.

September-October-November

For the period of SON (Figs. 3.7efgh), the dry regions of northern and southern Africa displayed small positive biases at 7 am, generally below 2°C, which shifted to neutral to slightly negative biases by 3 pm, (typically less than -2°C). South America had mostly cool biases at 7 am with the exception of some stations over the highlands of Brazil which had positive biases ranging from 2°C to 4°C. The largest errors were observed at 3 pm in the central Amazon, reaching up to 6°C in a few locations especially in 2023 and 2024 (Appendix, Figs. 5.7h and 5.9h). In Africa there were a few stations with biases of -4°C at both 7 am and 3 pm but these larger biases were isolated and not similar to those of nearby stations.

3.3.2 Dew Points

Median dewpoint biases at each weather station for each season combining data for the three years are shown in Figures 3.8 and 3.9. For context, similar information but separated into each 3 month season for each year is presented in Appendix Figures 5.10 to 5.15.

Across both Africa and South America, the GFS model shows a consistent dry bias in dew point forecasts in all seasons in most climate zones (Figs. 3.8abcdefgh and 3.9abcdefgh). This dry tendency is stronger during the rainy seasons (Table 3.5), suggesting that the model may struggle to accurately represent atmospheric moisture when precipitation is frequent and surface moisture is high. The strongest biases are found in tropical and subtropical regions where rainfall is more frequent, while some neutral conditions occur in drier or cooler regions during their respective dry seasons.

December-January-February

During the DJF season throughout the 3-year period (2022-2024), both 7 am and 3 pm dew points are dry in almost all parts of Africa, with the exception of the coasts of North Africa and South Africa, where median biases are mostly neutral or slightly wet (around 2°C). West and Central Africa have the largest dry biases, exceeding 6°C, which coincides with their rainy season (Appendix, Figs. 5.10ab, 5.12ab, 5.14ab). South America also shows widespread dry biases during DJF, particularly in the afternoon (Appendix, Figs. 5.10cd, 5.12cd, 5.14cd). However, a few stations in the southern part of Brazil show neutral to slightly wet median values at 3 pm.

March-April-May

MAM shows a similar pattern to DJF. In Africa, the strongest dry biases again appear in West and Central Africa, with median values greater than 6°C (Appendix, Figs. 5.10ef, 5.12ef, 5.14ef). These regions also experience frequent rainfall during this season. In South America, GFS dew points remain dry at both times of day, except in a few stations located in mountainous areas in the west and east of the continent within the Andes and highlands of Brazil (Appendix, Figs. 5.10gh, 5.12gh, 5.14gh).

June-July-August

In JJA, the magnitude of dry biases decreases across both continents compared to MAM except in the tropical climate zones where large dry biases in the 4 – 6°C range occur in the afternoon. In Africa, most stations have 2–4°C dry median biases especially in the morning, and fewer stations in North Africa show moist biases compared to earlier seasons (Appendix, Figs. 5.11ab, 5.13ab, 5.15ab). In South America, GFS performs better in Southern regions where median dew point biases are mostly neutral to slightly positive (0 to 2°C), especially in 2022 (Appendix, Figs. 5.11cd, 5.13cd, 5.15cd).

September-October-November

During SON, afternoon (3 pm) dew point biases are noticeably drier than morning (7 am) across both continents than in JJA. In Africa, North Africa is almost neutral in the morning, but other regions show afternoon biases exceeding 6°C, while morning biases are mostly under 4°C (Appendix, Figs. 5.11ef, 5.13ef, 5.15ef). South America displays a similar diurnal difference, with dry afternoon conditions dominating most regions, except for southern South America, which remains mostly neutral (Appendix, Figs. 5.11gh, 5.13gh, 5.15gh).

3.3.3 Discussion

Dew point biases of only a few degrees can have large impacts on instability and the likelihood of storm development. To assess the sensitivity of CAPE to low-level moisture, dewpoints below 900 hPa were systematically increased and decreased by 2°C in for example profiles from Angola (Fig. 3.10abc) and Brazil (Fig. 3.10def). A ±2°C modification in near-surface dewpoints leads to a significant changes in CAPE. For the Angola example profile, CAPE decreased from 845 J/kg to 213 J/kg when dewpoints were reduced by 2°C, and increased to 1608 J/kg when dewpoints were raised by 2°C. For the Brazil example profile , CAPE decreased from 2490 J/kg to 975 J/kg when dewpoints were reduced by 2°C, and increased to 3751 J/kg when dewpoints were raised by 2°C. These results demonstrate that a 2°C dewpoint bias can result in more than a one-third difference in CAPE and this can potentially impact prediction of storms and daily precipitation.

Kennedy (2023) examined air temperature and dew point biases at stations in North America for the GFS and the Navy's Coupled Ocean/Atmosphere Mesoscale Prediction System model (COAMPS) regional model. Her analysis revealed that 48-hour leadtime temperature and dew point forecasts from both models showed a clear regional and diurnal patterns (Fig. 3.11). North American summer is more comparable to tropical and subtropical conditions than winter.

During summer, North American temperature biases were generally smaller ranging from approximately < ±4°C with most values ranging within ±2°C. These results are consistent with findings from Patel et al. (2021). In contrast,temperature biases in Africa and South America reached up to < ±6°C across all seasons, with some regions exceeding exceeding 6°C.

North American dew point biases (Figure 3.12) primarily range from 0°C to –4°C, indicating a consistent dry tendency across the region. This dry pattern is also seen in Africa and South America, where dew point biases were mainly negative, with some areas exceeding –6°C. All three continents share a predominantly dry trend, but Africa and South America exhibit larger and more variable negative biases, compared to the more uniform and moderate dry biases in North America. Additionally, dew point biases in South America displayed a generally wider distribution than those in Africa.

Overall, our analysis revealed that GFS temperature and dew point biases in Africa and South America vary geographically and seasonally. Afternoon air temperatures tend to be under forecast in the Cool West Temperate zone for both continents and for the Tropical climate zone in Africa. The most concerning findings are the dry dew point biases across all climate zones and seasons (Figs. 3.1cd, 3.8 - 3.9). The consistency of the too dry dewpoints for Africa, South America, and North America suggests that GFS model may be underestimating near surface humidity due to issues in representing evaporation (including vegetation cover and evapotranspiration), soil moisture, mixing processes in the boundary layer, or advection of moister air masses.

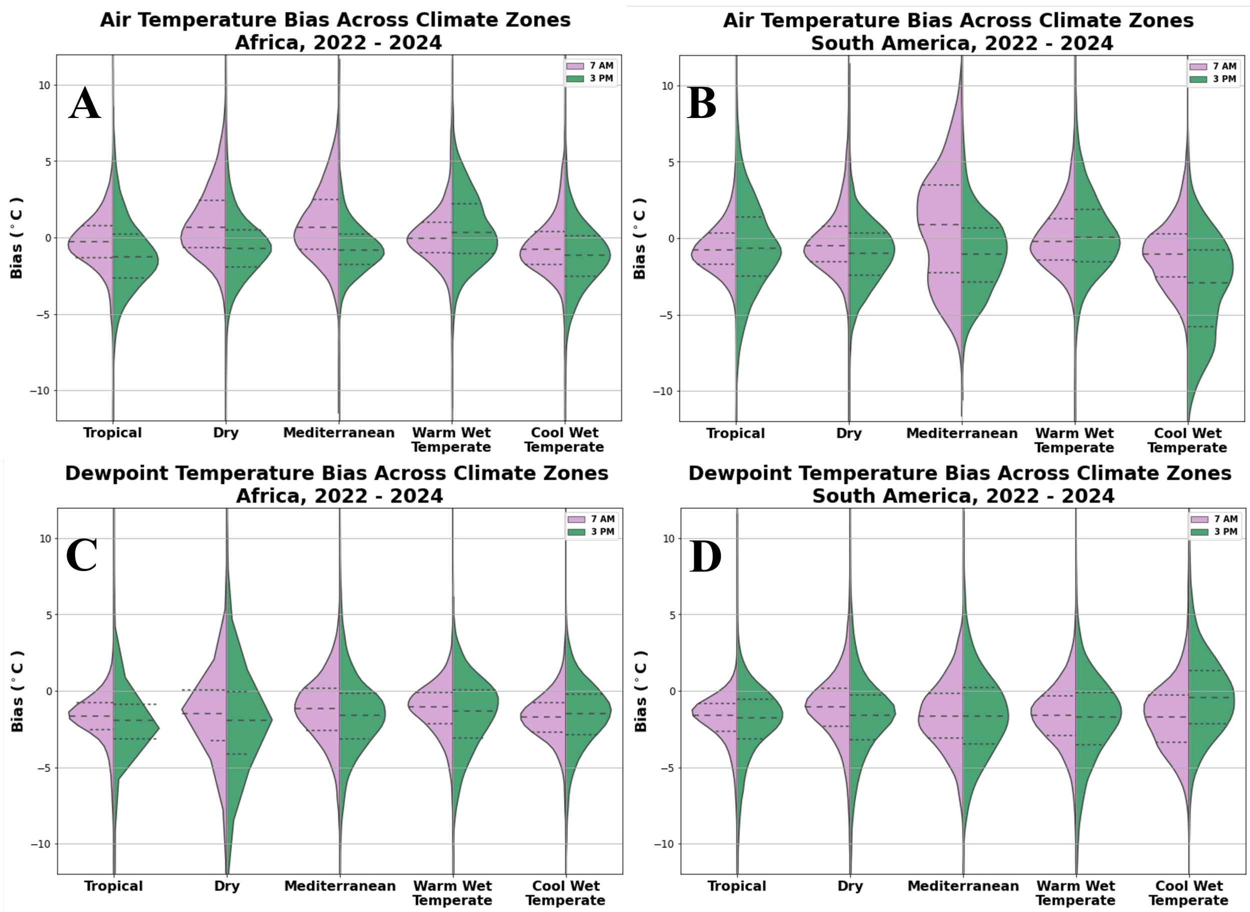

Figure 3.1: Violin plots detailing the annual distributions of GFS ∼48hr leadtime air temperature and dew point errors at 7 AM (plum) and 3 PM (mediumseagreen) across climate zones in Africa (A and C) and South America (B and D) combining the 4 seasons from 2022 through 2024. Dashed lines corresponds to median value, dotted lines corresponds to 75th and 25th percentiles.

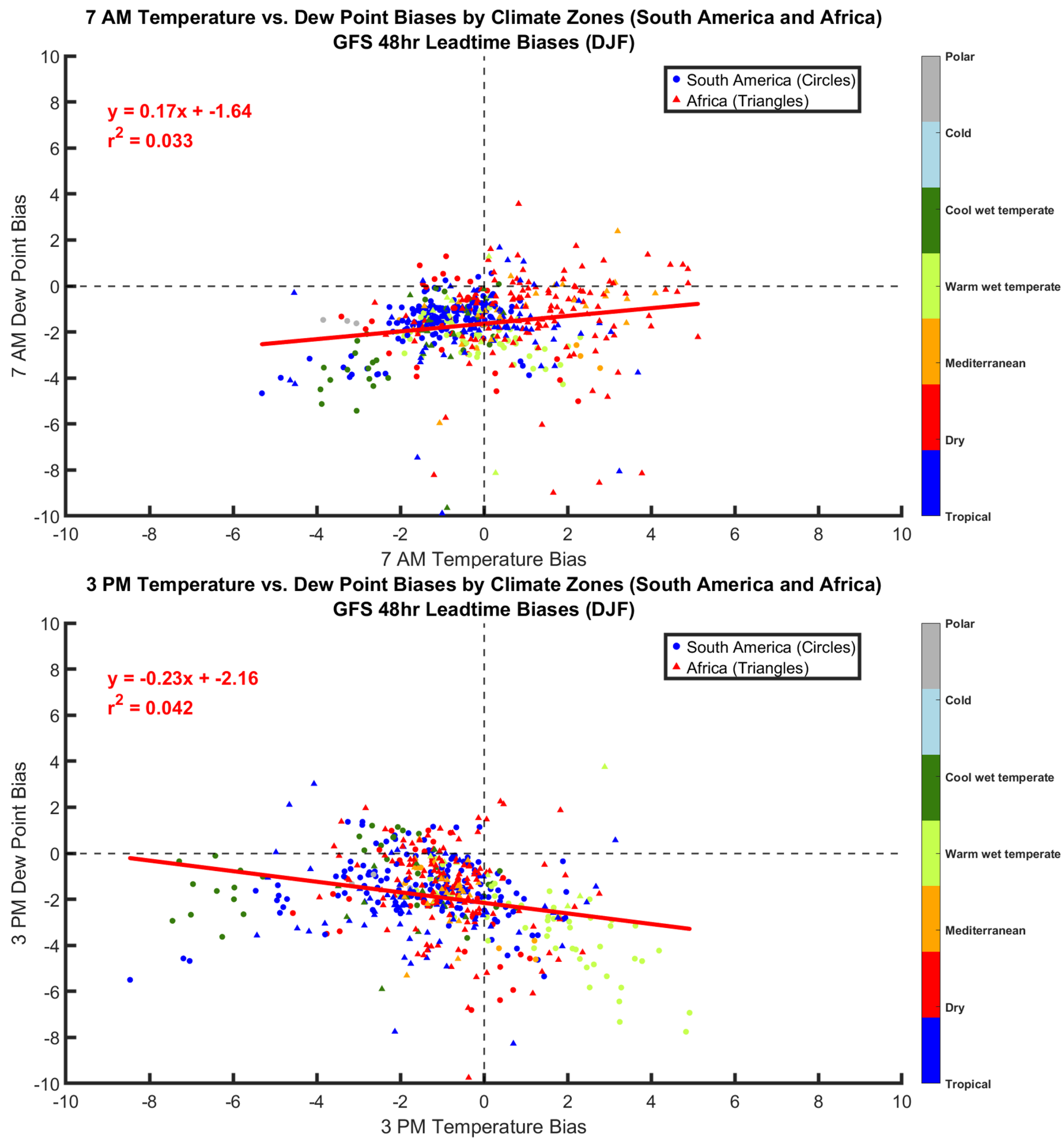

Figure 3.2: DJF season scatter plots of seasonal median air temperature bias vs dewpoint temperature bias for Africa (triangle) and South America (circle) at 7 am and at 3 PM. In each plot, a single station is represented by three points, one each for DJF 2022, DJF 2023, and DJF 2024. Symbols are color-coded by climate zone. A linear regression line is included in each plot to highlight the overall relationship between temperature and dew point biases, along with the correlation coefficient (r^2) to indicate the strength of the relationship.

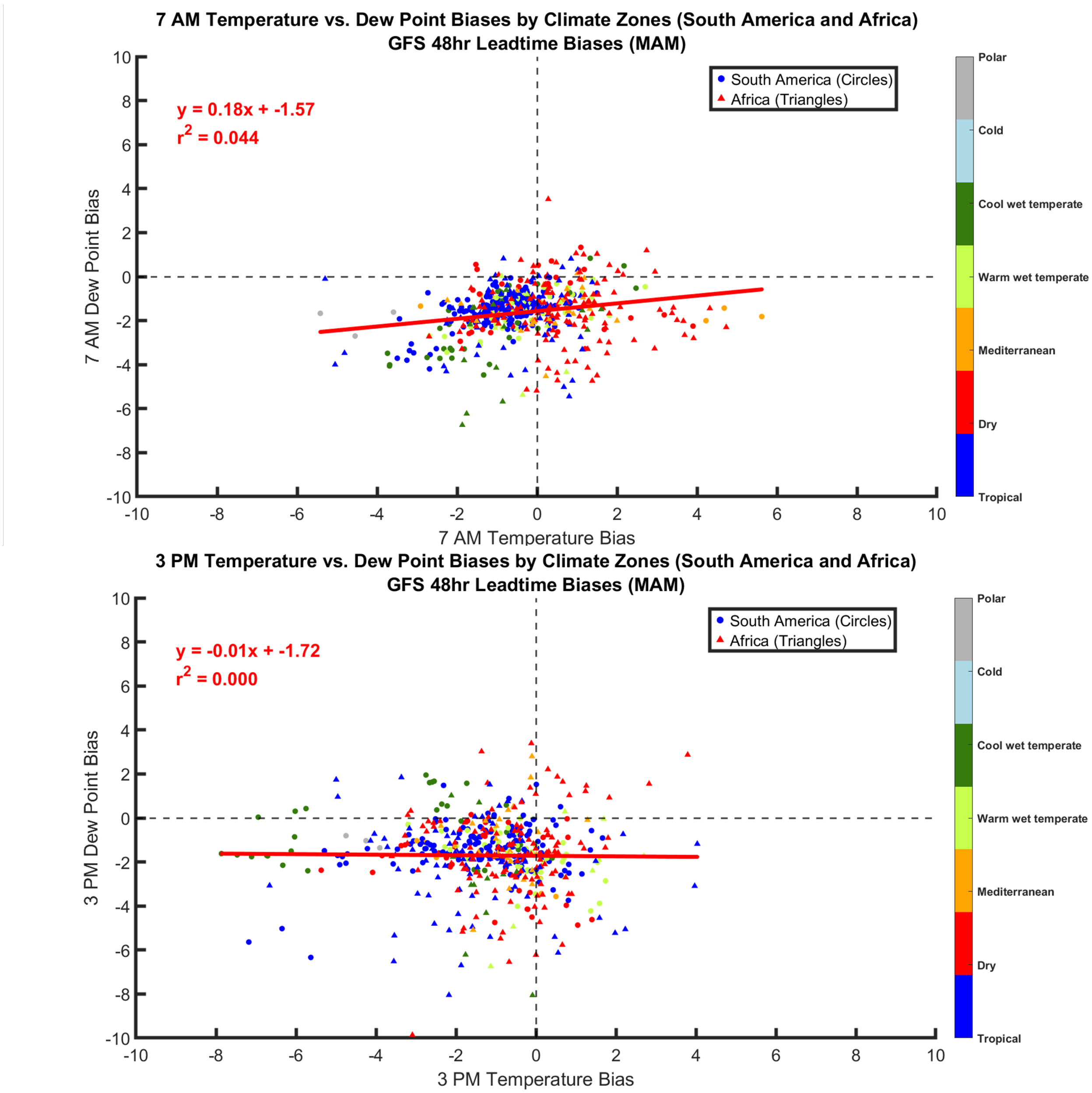

Figure 3.3: MAM season scatter plots of seasonal median air temperature bias vs dewpoint temperature bias for Africa (triangle) and South America (circle) at 7 am and at 3 PM. In each plot, a single station is represented by three points, one each for MAM 2022, MAM 2023, and MAM 2024. Symbols are color-coded by climate zone. A linear regression line is included in each plot to highlight the overall relationship between temperature and dew point biases, along with the correlation coefficient (r^2) to indicate the strength of the relationship.

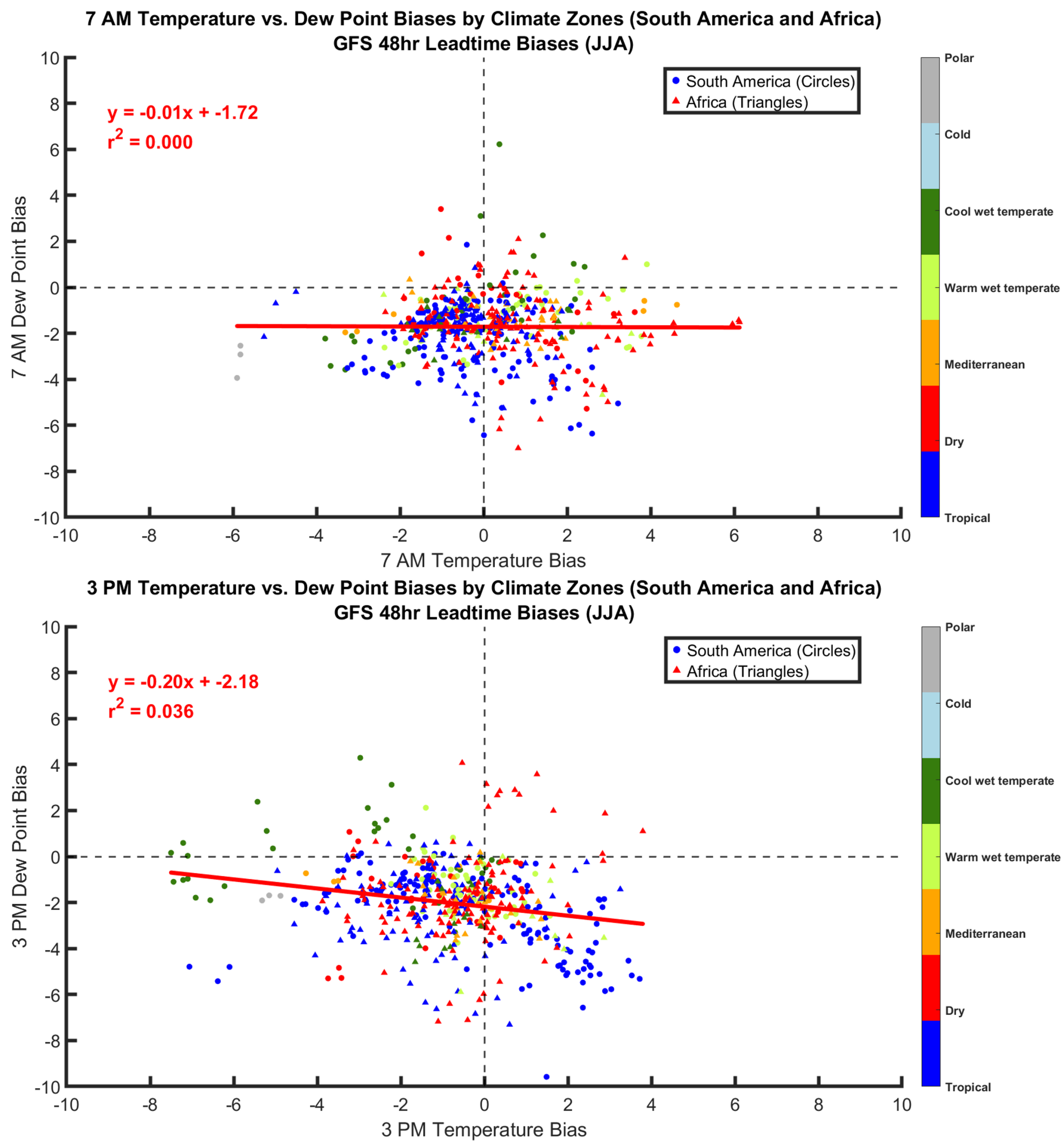

Figure 3.4: JJA season scatter plots of seasonal median air temperature bias vs dewpoint temperature bias for Africa (triangle) and South America (circle) at 7 am and at 3 PM. In each plot, a single station is represented by three points, one each for JJA 2022, JJA 2023, and JJA 2024. Symbols are color-coded by climate zone. A linear regression line is included in each plot to highlight the overall relationship between temperature and dew point biases, along with the correlation coefficient (r^2) to indicate the strength of the relationship.

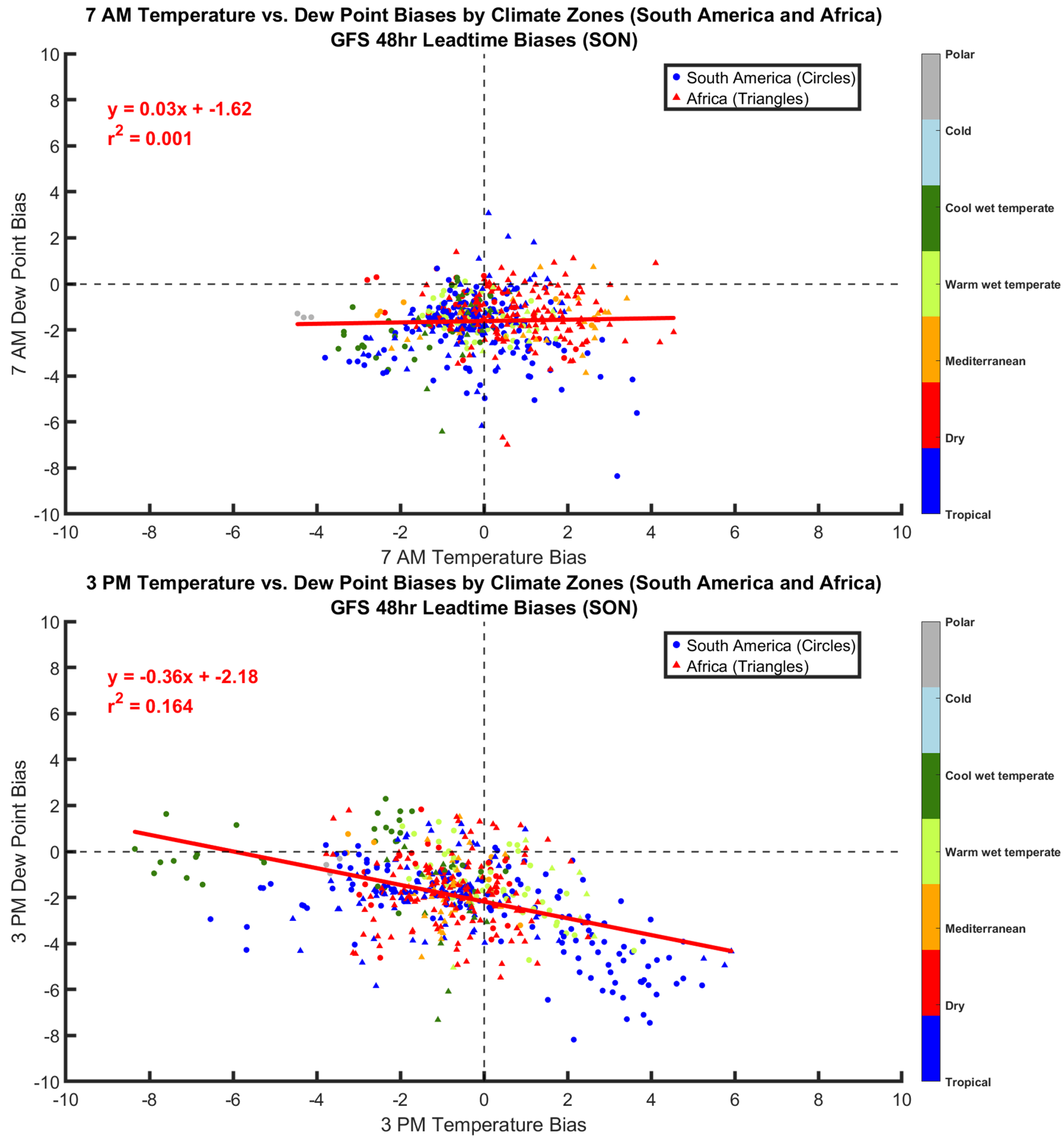

Figure 3.5: SON season scatter plots of seasonal median air temperature bias vs dewpoint temperature bias for Africa (triangle) and South America (circle) at 7 am and at 3 PM. In each plot, a single station is represented by three points, one each for SON 2022, SON 2023, and SON 2024. Symbols are color-coded by climate zone. A linear regression line is included in each plot to highlight the overall relationship between temperature and dew point biases, along with the correlation coefficient (r^2) to indicate the strength of the relationship.

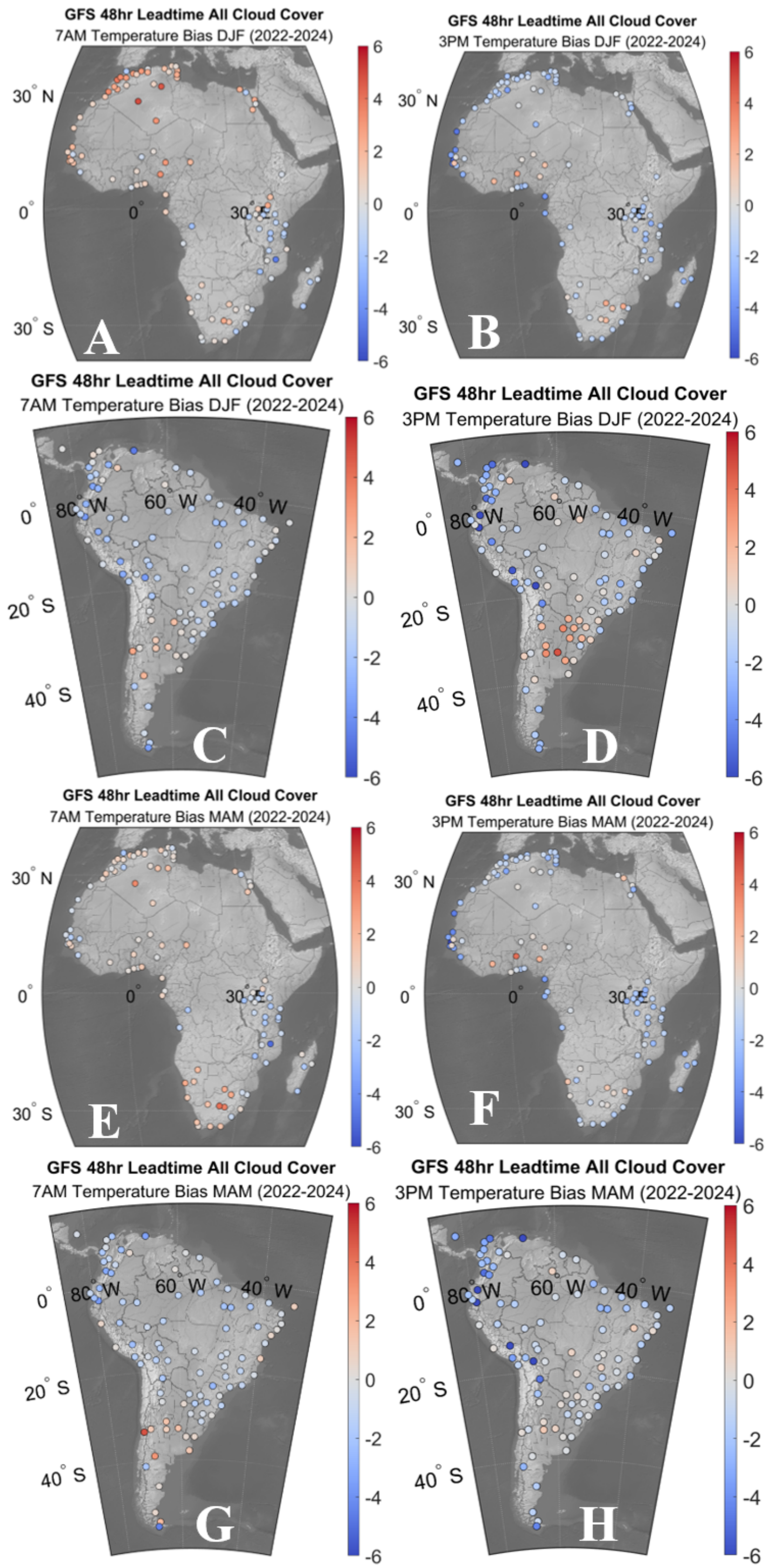

Figure 3.6: Geographical Map of Median Temperature Biases for DJF and MAM seasons for a 3 - year period (2022-2024)

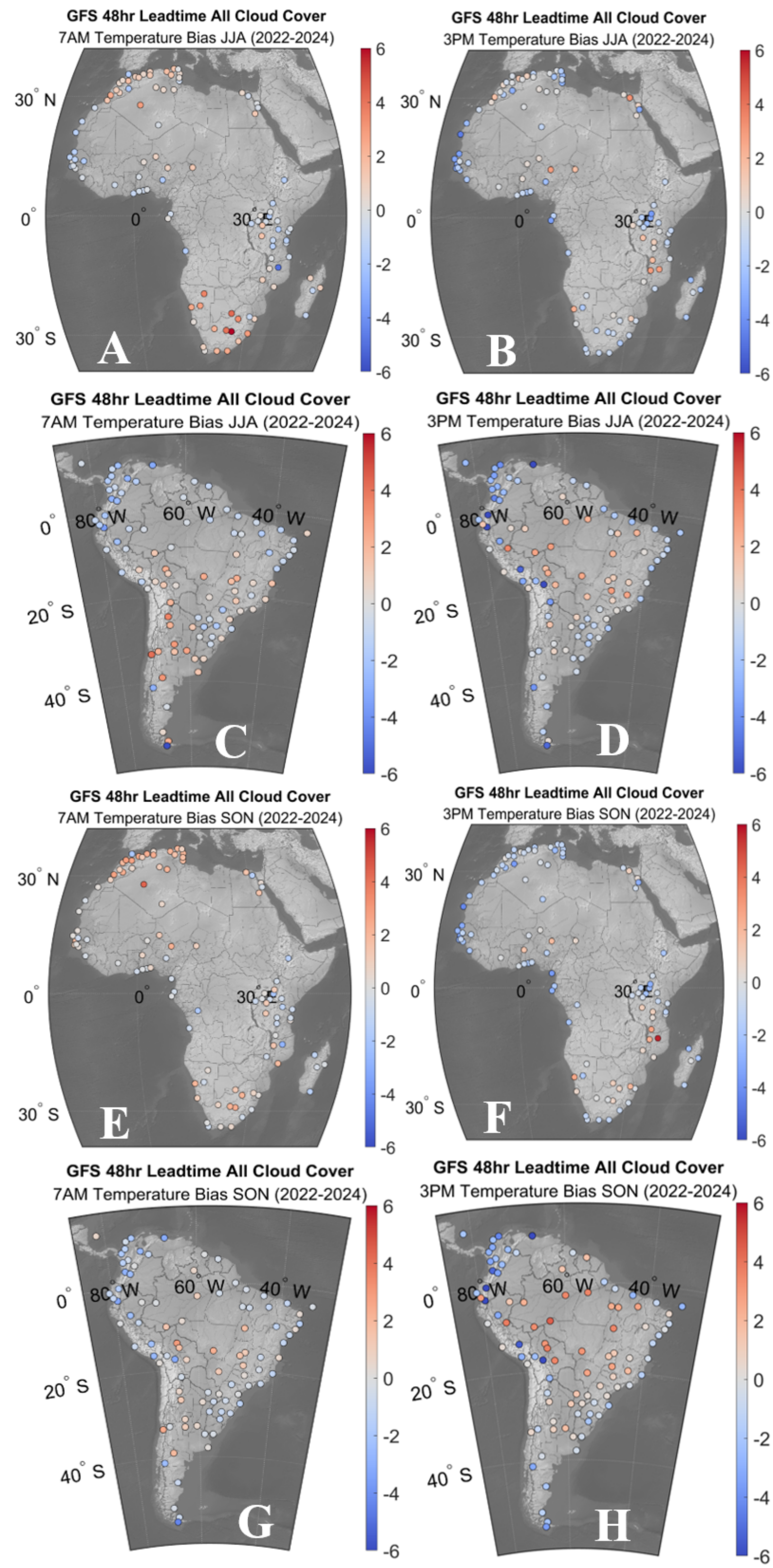

Figure 3.7: Geographical Map of Median Temperature Biases for JJA and SON seasons for a 3 - year period (2022-2024)

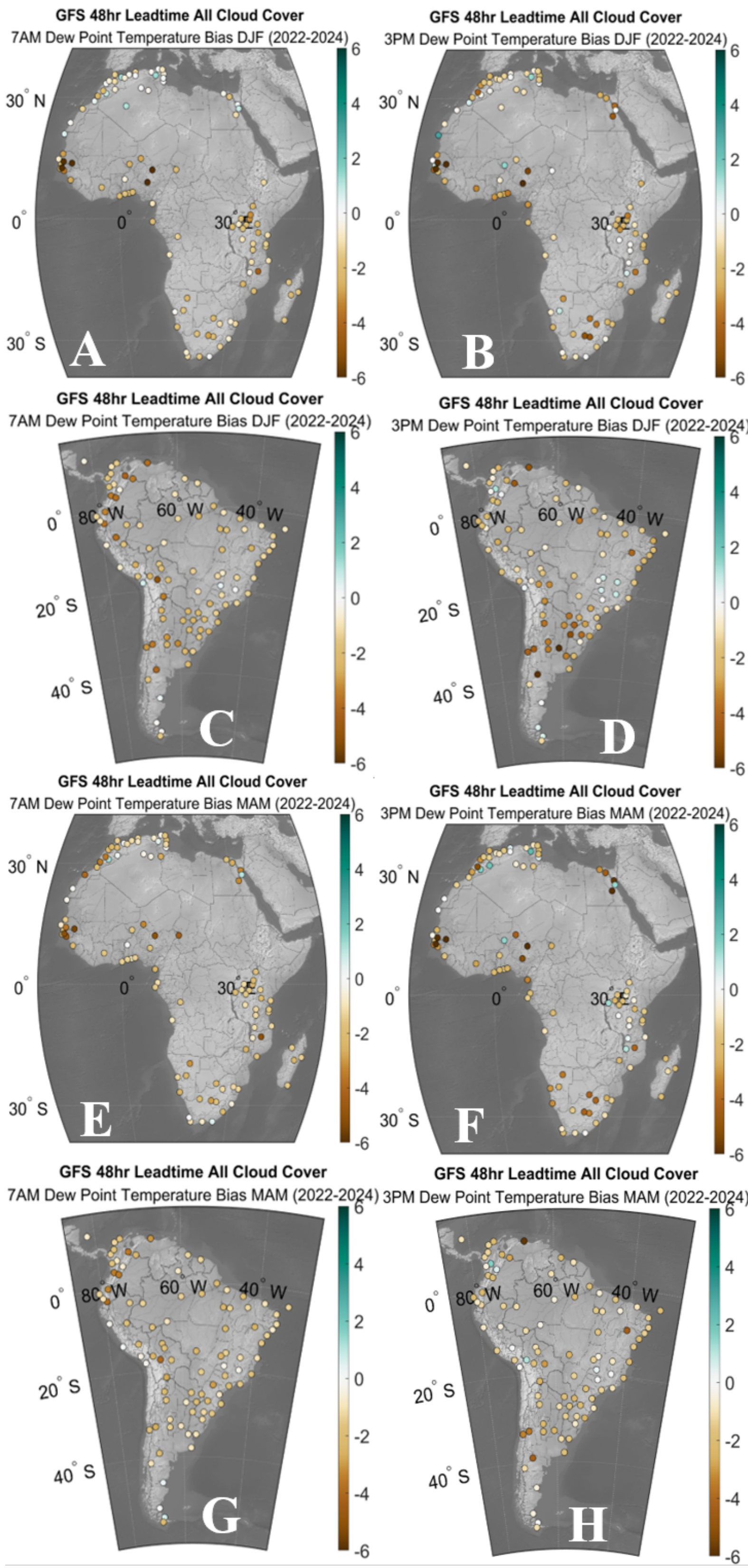

Figure 3.8: Geographical Map of Median Dewpoints Biases for DJF and MAM seasons for a 3 - year period (2022-2024)

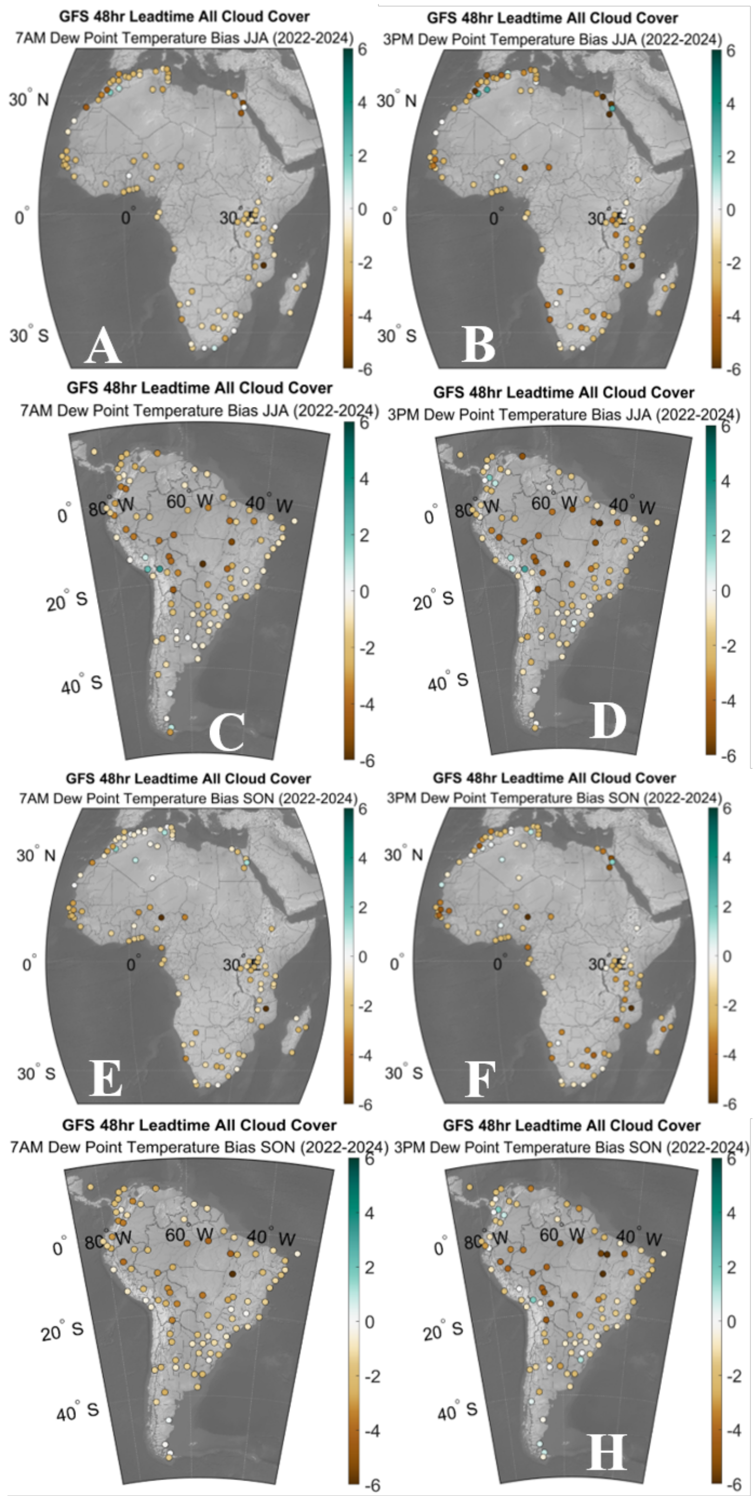

Figure 3.9: Geographical Map of Median Dewpoints Biases for JJA and SON seasons for a 3 - year period (2022-2024)

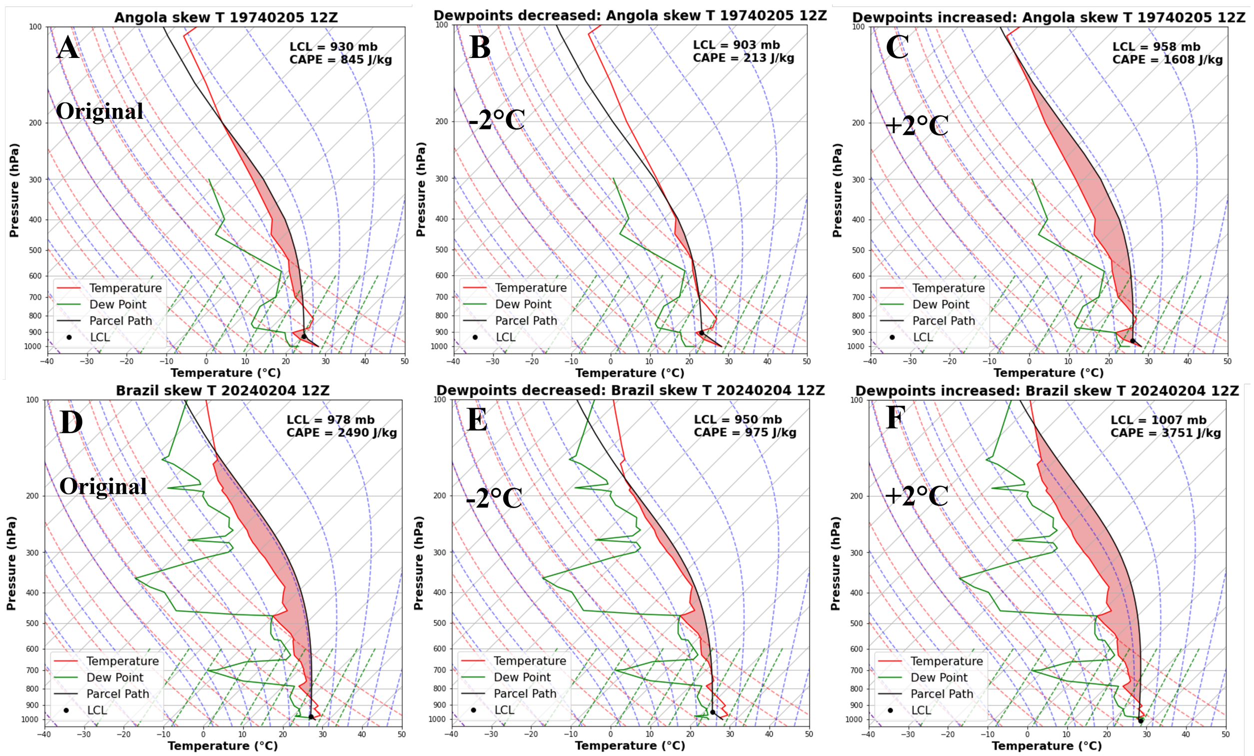

Figure 3.10: Skew-T diagrams for Luanda, Angola A), B) and C) on 2 May 1974 at 12Z and Manaus, Brazil D), E) and F) on 2 April, 2024 at 12Z showing how changes in near surface dewpoint temperatures affect CAPE. A) and D) show the observed soundings. In the modified soundings, the first four levels corresponding to the lowest ∼100 hPa are adjusted in B) and E) to reduce dewpoints by -2°C and in C) and F) to increase dewpoints by +2°C. CAPE is annotated in red shading. CAPE and LCL values are shown in the upper right of each plot.

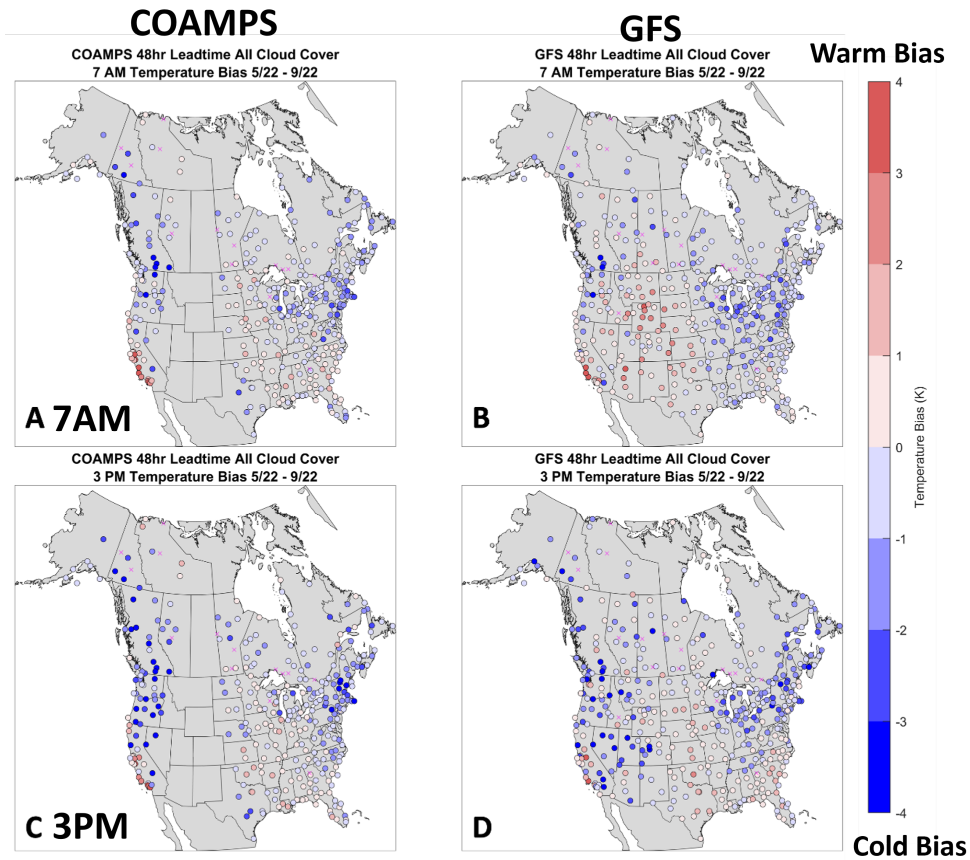

Figure 3.11: Summer season air temperature biases between weather station observations and 48-hourish leadtime forecasts from Navy's COAMPS regional model (left column) and NOAA GFS for North America for period May 2022 - September 2022 at 7 am local time (top row) and 3 pm local time (bottom row). Adapted from Kennedy (2023).

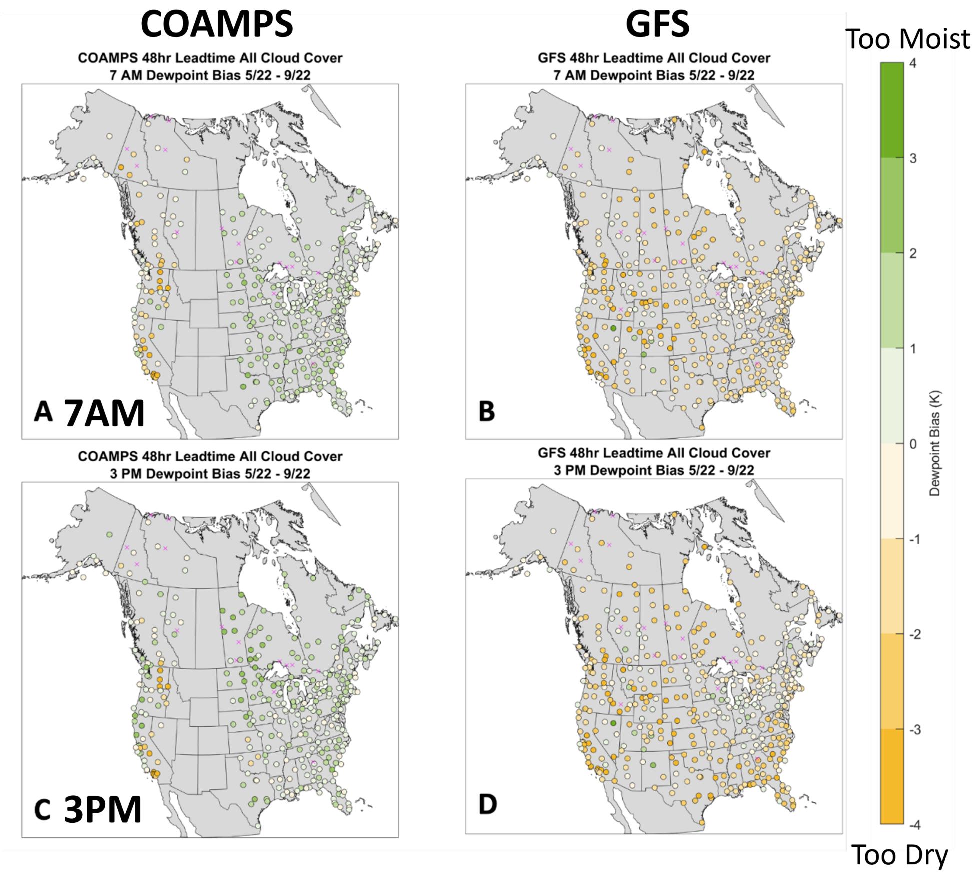

Figure 3.12: Summer season air temperature biases between weather station observations and 48-hourish leadtime forecasts from Navy's COAMPS regional model (left column) and NOAA GFS for North America for period May 2022- September 2022 at 7 am local time (top row) and 3 pm local time (bottom row). Adapted from Kennedy (2023).

CHAPTER

4

CONCLUSIONS

This study examines GFS forecast biases in air temperature and dew point for Africa and South America, regions that have not been systematically addressed in previous evaluations of GFS performance. The analysis focuses on approximately 48-hour lead time forecasts and compares matched weather station observations with model forecasts at 7 AM local time (corresponding to approximate diurnal minimum temperature) and 3 PM (corresponding to approximate diurnal maximum temperature). Information on the strengths and weaknesses of GFS forecasts across different climate zones is intended to aid users of these forecasts outside of the US to assess their relative reliability. The analysis used over 200,000 hourly data points collected from 105 stations in Africa and 98 stations in South America, across 7 simplified climate zones on both continents (Tropical, Dry, Mediterranean, Warm Wet Temperate, Cool Wet Temperate, Cold , and Polar).

We considered that annual median biases < ±1°C and 10th or 90th percentile biases < ±5°C were within a reasonable margin of error. There was no strong covariance between dew points and air temperature biases for a given season at the same local times (Sec. 3.2.1, and Figs. 3.2, 3.4, 3.3 and 3.5). Hence, dew point biases and temperature biases are not a simple function of one another. The key weaknesses for GFS in Africa and South America are:

- GFS is systematically forecasting dew points that are too dry at 7 am and 3 pm local time (more than 1°C in annual median) across nearly all climate zones (Tables 3.3 and

3.4). Dry biases can exceed 4°C in specific locations seasonally (Figs. 3.8 and 3.9). The most severe dry biases occur during the wet seasons (Sec. 3.2.1). This consistent dry bias suggests that GFS model is struggling in the representation of atmospheric moisture and land–atmosphere interactions.

- GFS under forecasts afternoon air temperatures (more than 1°C in annual median) in Tropical climate zone in Africa and Cool Wet Temperate climate zones in both Africa and South America. The largest negative biases at individual weather stations are most common during SON at 3 pm local time. (Tables 3.1 and 3.2, Fig. 3.5).
- When the biases for individual weather stations were aggregated, there were longer tails in the temperature bias distributions for South America as compared to Africa (Figs. 5.1, 5.2 and 5.3). This may be a result of a few more major cities in South America (and their associated airport weather stations) being located in complex and/or elevated terrain than in Africa.

National weather services in Africa and South America should be cautious in using GFS to forecast dew points at any time of year. To compensate, local forecasters should up GFS forecast values by a few degrees. Too dry dew points have several potential feedbacks which could yield underestimates of low altitude cloud cover, surface-based instability, and precipitation amounts.

Most of the median annual air temperature biases are less than 1°C but tend to be a bit larger in the afternoon than morning and are larger seasonally in DJF, MAM, and SON as compared to JJA (Sec. 3.1.1 and 3.2.1). A correction could be made depending on the local conditions and the amount of rainfall (during DJF, MAM,and SON it is generally wet in most parts of Tropics) to be able to increase the accuracy of the temperature forecasts.

Specifically for Tanzania, it is recommended to increase GFS predicted dewpoint temperatures by 2°C throughout the year as the model consistently underestimates atmospheric moisture. For air temperature, seasonal adjustments of +1°C are recommended during DJF and MAM seasons. In JJA, it is suggested that GFS air temperature forecasts be decreased by 1°C.

Examination of forecast biases outside of the US is worthwhile to improve understanding of GFS strengths and weaknesses in different environments. Similar to the findings of too dry dewpoints for Africa and South America, for North America Kennedy (2023) found that summer (May-Sept) dew point forecasts for GFS were also too dry at both 7 am and 3 pm (Fig. 3.12). Compared to Africa and South America, air temperature bias results for North America summer had a smaller range of values and distinct regional variations between cold and warm biases (Fig. 3.11). As described in Chapter 3, the under estimation of dew point could be the result of one or several issues including how the GFS model is representing evaporation, vegetation cover and evapotranspiration, soil moisture, mixing processes in the boundary layer, and/or advection of moister air masses. Untangling these will be complicated. Additional investigation of the sensitivity of the biases to amount of cloud cover and to the onset and end of the wet seasons would be helpful in constraining the likely physical processes that need refinement in GFS. Hourly sky cover data based on surface observations is available for some stations in Africa and South America. Analysis of satellite datasets will be needed to thoroughly evaluate whether there are systematic biases in GFS forecasts of cloud cover and is beyond the scope of this thesis.

This study focused on raw GFS 2-meter forecasts. Future work could evaluate bias-corrected products like GFS - Model Output Statistics (MOS), which apply statistical post-processing to improve forecast accuracy. However, GFS-MOS products are currently only available for the United States and parts of Canada, as noted by Charba and Samplatsky (2011).

REFERENCES

Ahrens, C. D., and R. Henson, 2018: *Meteorology Today: An Introduction to Weather, Climate and the Environment*. 12th ed., Cengage Learning, Boston, MA.

Berntell, E., 2023: Understanding west african monsoon variability: Insights from paleoclimate modeling of past warm climates. Ph.D. thesis, Stockholm University, Stockholm, Sweden, URL https://su.diva-portal.org/smash/record.jsf?pid=diva2%3A1752119&dswid=-2875.

Biasutti, M., M. Ting, and S. A. Hill, 2023: The dynamics and changes of the world's monsoons. *Physics Today*, **76 (9)**, 32–38, https://doi.org/10.1063/PT.3.5308, URL https://pubs.aip.org/physicstoday/article/76/9/32/2908397/The-dynamics-and-changes-of-the-world-s.

Charba, J. P., and F. G. Samplatsky, 2011: Regionalization in Fine-Grid GFS MOS 6-h Quantitative Precipitation Forecasts. *Monthly Weather Review*, **139 (1)**, 24–38, https://doi.org/10.1175/2010MWR2926.1, URL http://journals.ametsoc.org/doi/10.1175/2010MWR2926.1.

Hagos, S. M., and K. H. Cook, 2005: Influence of Surface Processes over Africa on the Atlantic Marine ITCZ and South American Precipitation. *Journal of Climate*, **18 (23)**, 4993–5010, https://doi.org/10.1175/JCLI3586.1.

Hohenegger, C., P. Brockhaus, C. S. Bretherton, and C. Schär, 2009: The Soil Moisture-Precipitation Feedback in Simulations with Explicit and Parameterized Convection. *Journal of Climate*, **22 (19)**, 5003–5020, https://doi.org/10.1175/2009JCLI2604.1.

Huete, A., K. Didan, T. Miura, E. P. Rodriguez, X. Gao, and L. G. Ferreira, 2002: Overview of the radiometric and biophysical performance of the MODIS vegetation indices. *Remote Sensing of Environment*, **83 (1-2)**, 195–213, https://doi.org/10.1016/S0034-4257(02)00096-2.

Kennedy, R., 2023: Assessing Numerical Weather Prediction Model Forecast Skill Under Different Weather Conditions Using Surface Observations. M.S. thesis, North Carolina State University, Raleigh, NC, URL https://www.lib.ncsu.edu/resolver/1840.20/41348.

Kottek, M., J. Grieser, C. Beck, B. Rudolf, and F. Rubel, 2006: World Map of the Köppen-Geiger Climate Classification Updated. *Meteorologische Zeitschrift*, **15**, 259–263, https://doi.org/10.1127/0941-2948/2006/0130.

Patel, R. N., S. E. Yuter, M. A. Miller, S. R. Rhodes, L. Bain, and T. W. Peele, 2021: The Diurnal Cycle of Winter Season Temperature Errors in the Operational Global Forecast System (GFS). *Geophysical Research Letters*, **48 (20)**, https://doi.org/10.1029/2021GL095101.

Rouse, W., R. H. Haas, and W. Deering, 1974: Monitoring vegetation systems in the Great Plains with ERTS. *Earth Resources And Remote Sensing*, **1**, 309–317.

Yang, F., and R. Treadon, 2020: Development and Evaluation of NCEP's Global Forecast System Version 16. URL https://ufs.epic-dev.noaa.gov/2020/10/development-and-evaluation-of-nceps-global-forecast-system-gfsv16/.

CHAPTER

5

SUPPLEMENTAL INFORMATION

Table 5.1: Summary of the key physical parameterizations and model components used in the NOAA Global Forecast System (GFS), including grid spacing, convection schemes, turbulence, radiation, land surface, and soil moisture treatments.

NOAA GFS MODEL	
Grid Spacing	~27.5km (0.25 deg)
Cumulus Parameterization	SAS-based mass flux
Shallow Convection	SAS-based mass flux Shallow convection
PBL/Turbulent Mixing	Hybrid EDMF PBL and Free atmospheric Turbulence
Microphysics	GFDL (sa)
Surface Layer	GFS
Radiation (short/long wave)	RRTMG
Land surface	NOAH LSM
Soil moisture	NOAH LSM

Table 5.2: Summary statistics by climate zone for Africa air temperature bias including the 10th, 25th, 50th, and 90th percentiles. Under column for a 3-year period percentile average values (2022-2024). Highlighted in color are values with a median biases > ±1°C and 10th or 90th percentile biases > ±5°C.

Climate Zone	10th	25th	**50th**	75th	90th
Tropical 7am	–2.4	-1.3	**-0.3**	0.8	2.0
Tropical 3pm	-4.0	-2.6	**-1.3**	0.2	2.1
Dry 7am	-1.8	-0.7	**0.6**	2.4	4.4
Dry 3pm	-3.2	-1.9	**-0.7**	0.5	2.0
Mediterranean 7am	-2.0	-0.3	**0.7**	2.5	4.3
Mediterranean 3pm	-2.7	-1.8	**-0.8**	0.2	1.4
Warm Wet Temperate 7am	-2.0	-1.0	**0.1**	0.3	2.3
Warm Wet Temperate 3pm	-2.1	-1.0	**0.4**	2.2	3.9
Cool Wet Temperate 7am	-2.7	-1.7	**-0.8**	0.4	1.9
Cool Wet Temperate 3pm	-4.0	-2.5	**-1.2**	0.1	1.4

Table 5.3: Summary statistics by climate zone for South America air temperature bias including the 10th, 25th, 50th, and 90th percentiles. The average values (2022-2024)for a 3-year period percentile are shown in each column. Highlighted in color are values with a median biases > ±1°C and 10th or 90th percentile biases > ±5°C.

Climate Zone	10th	25th	**50th**	75th	90th
Tropical 7am	-2.6	-1.7	**-0.7**	0.3	1.5
Tropical 3pm	-4.5	-2.5	**-0.6**	1.4	3.5
Dry 7am	-2.6	-1.5	**-0.5**	0.7	2.6
Dry 3pm	-3.8	-2.4	**-1.0**	0.3	1.5
Mediterranean 7am	-4.3	-1.2	**0.9**	3.4	5.6
Mediterranean 3pm	-4.5	-2.9	**-1.1**	0.6	2.0
Warm Wet Temperate 7am	-2.4	-1.4	**-0.2**	1.2	2.9
Warm Wet Temperate 3pm	-3.0	-1.5	**0.0**	1.9	4.0
Cool Wet Temperate 7am	-3.8	-2.5	**-1.0**	0.3	1.8
Cool Wet Temperate 3pm	**-7.9**	-5.8	**-2.9**	-0.8	0.8

Table 5.4: Summary statistics by climate zone for Africa dew point bias including the 10th, 25th, 50th, and 90th percentiles. The average values (2022-2024)for a 3-year period percentile are shown in each column. Highlighted in color are values with a median biases > ±1°C and 10th or 90th percentile biases > ±5°C.

Climate Zone	10th	25th	**50th**	75th	90th
Tropical 7am	-3.9	-2.5	**-1.6**	-0.8	0.1
Tropical 3pm	**-5.0**	-3.1	**-1.7**	-0.9	0.5
Dry 7am	**-5.5**	-3.2	**-1.5**	0.0	1.7
Dry 3pm	**-6.7**	-4.2	**-2.0**	-0.0	2.1
Mediterranean 7am	-4.1	-2.6	**-1.2**	0.1	1.6
Mediterranean 3pm	-4.9	-3.1	**-1.6**	-0.2	1.5
Warm Wet Temperate 7am	-3.6	-2.2	**-1.0**	-0.1	0.9
Warm Wet Temperate 3pm	**-5.0**	-3.0	**-1.3**	0.0	1.2
Cool Wet Temperate 7am	-3.8	-2.7	**-1.7**	-0.8	0.2
Cool Wet Temperate 3pm	-4.4	-2.8	**-1.5**	-0.2	0.9

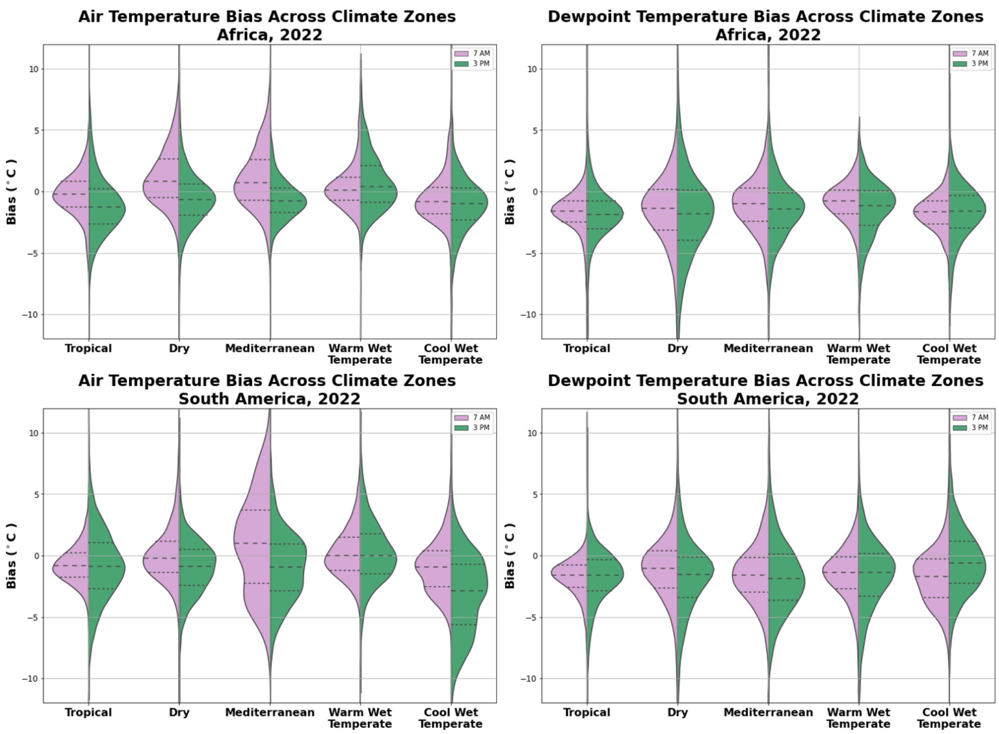

Figure 5.1: Violin plots detailing the annual distributions of GFS ~48hr leadtime air temperature and dew point errors at 7 AM (plum) and 3 PM (mediumseagreen) across climate zones in Africa and South America combining the 4 seasons in 2022. Dashed lines corresponds to median value, dotted lines corresponds to 75th and 25th percentiles.

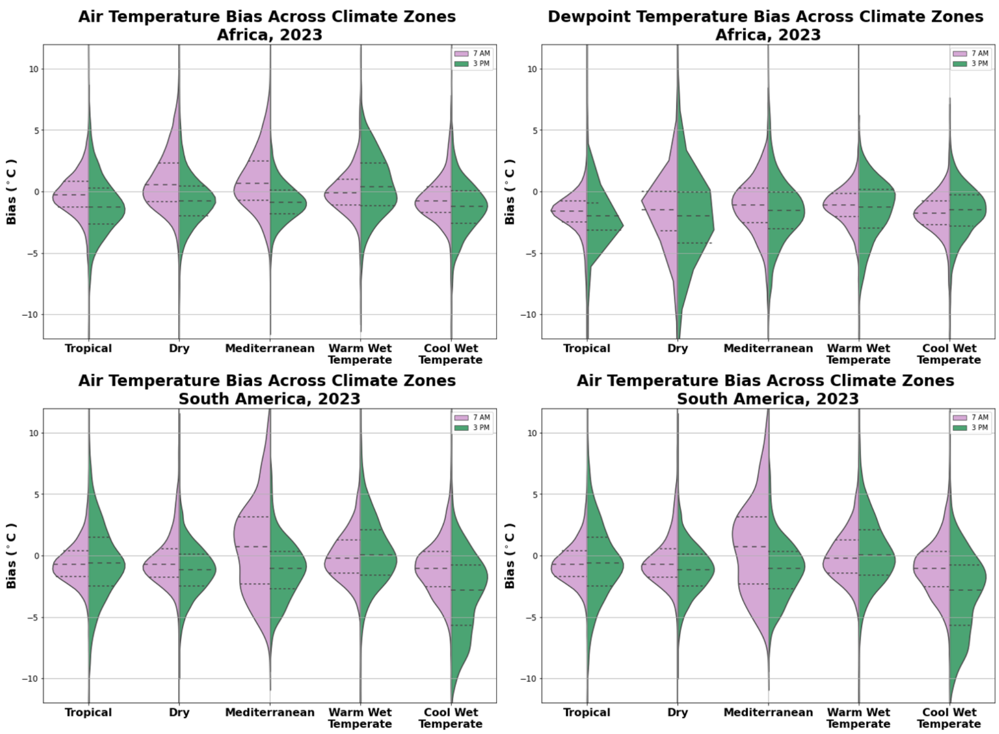

Figure 5.2: Violin plots detailing the annual distributions of GFS ∼48hr leadtime air temperature and dew point errors at 7 AM (plum) and 3 PM (mediumseagreen) across climate zones in Africa and South America combining the 4 seasons in 2023.Dashed lines corresponds to median value, dotted lines corresponds to 75th and 25th percentiles.

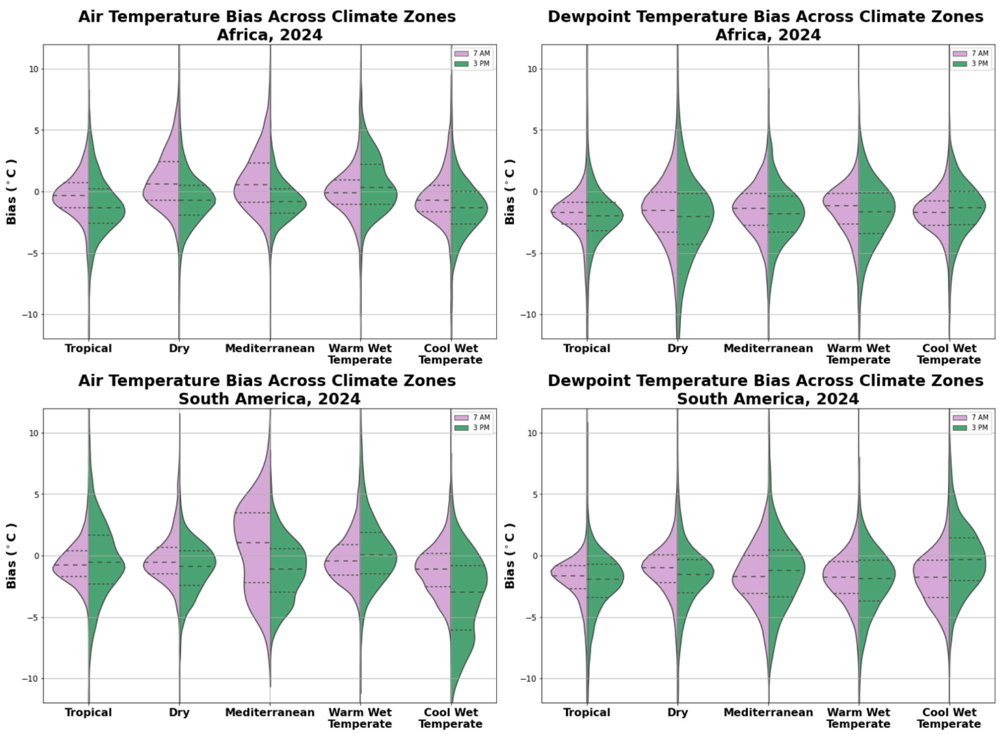

Figure 5.3: Violin plots detailing the annual distributions of GFS ∼48hr leadtime air temperature and dew point errors at 7 AM (plum) and 3 PM (mediumseagreen) across climate zones in Africa and South America combining the 4 seasons in 2024. Dashed lines corresponds to median value, dotted lines corresponds to 75th and 25th percentiles.

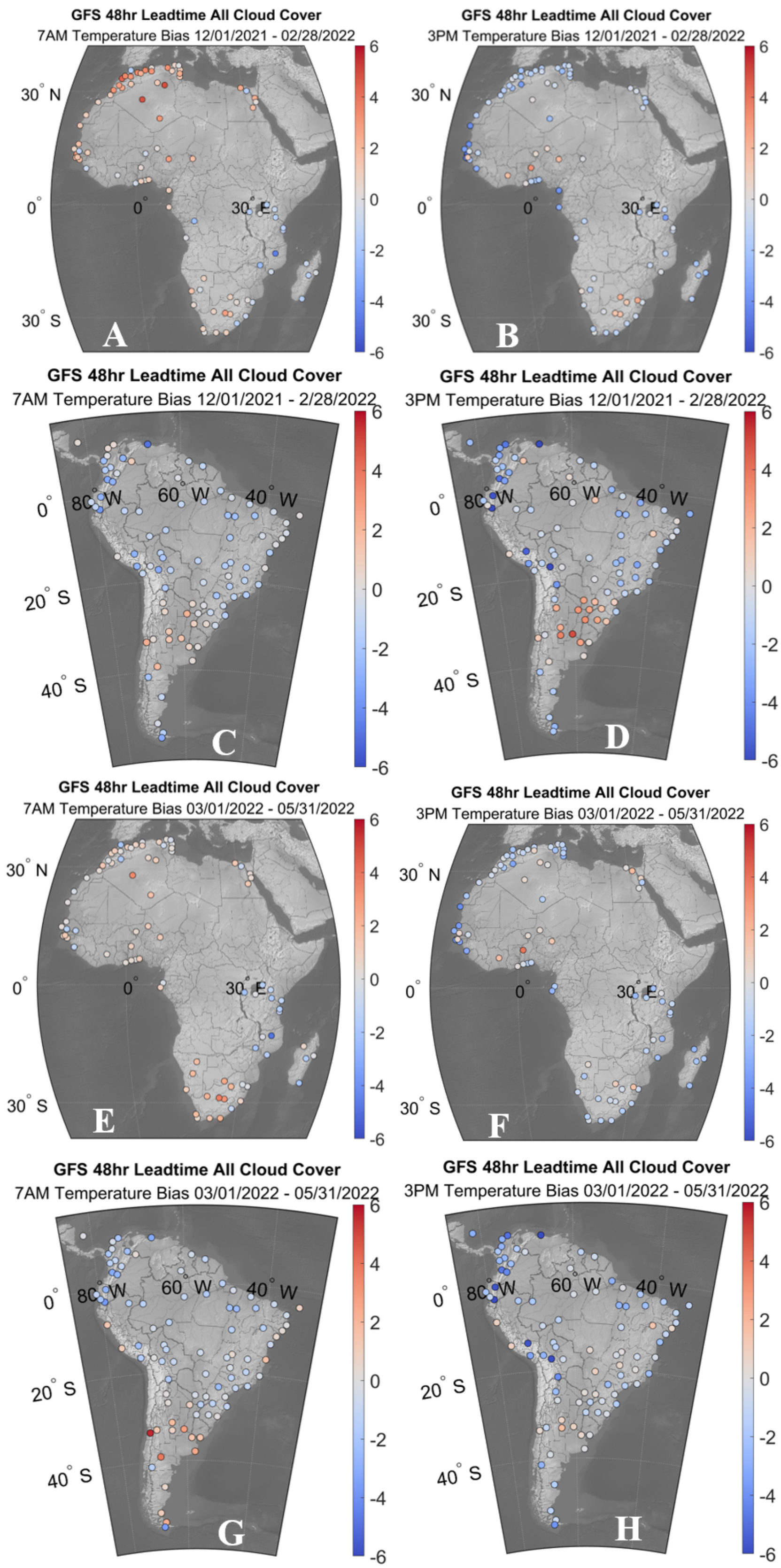

Figure 5.4: Geographical Map of Median Temperature Biases for DJF and MAM seasons, 2022

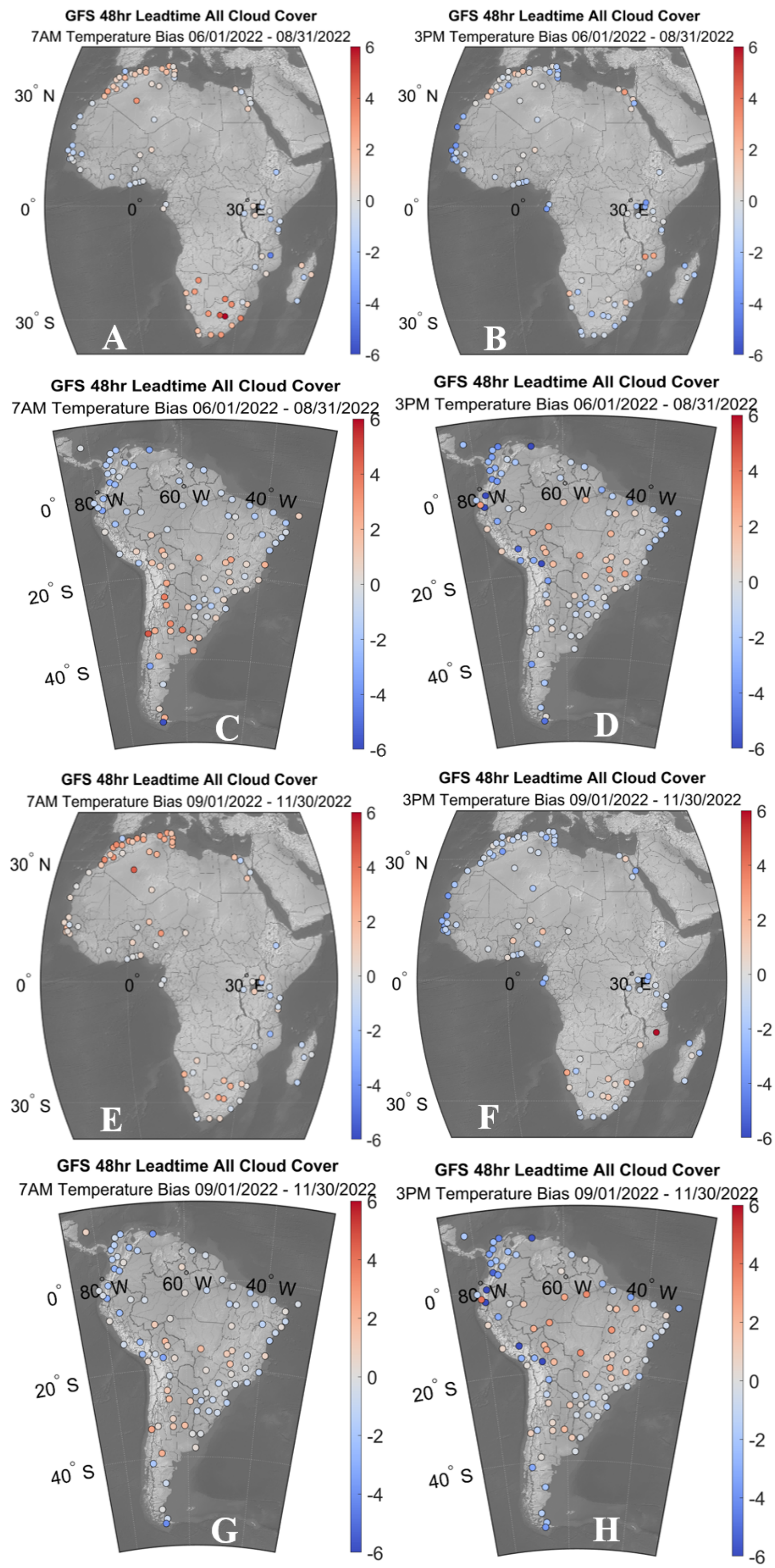

Figure 5.5: Geographical Map of Median Temperature Biases for JJA and SON seasons, 2022

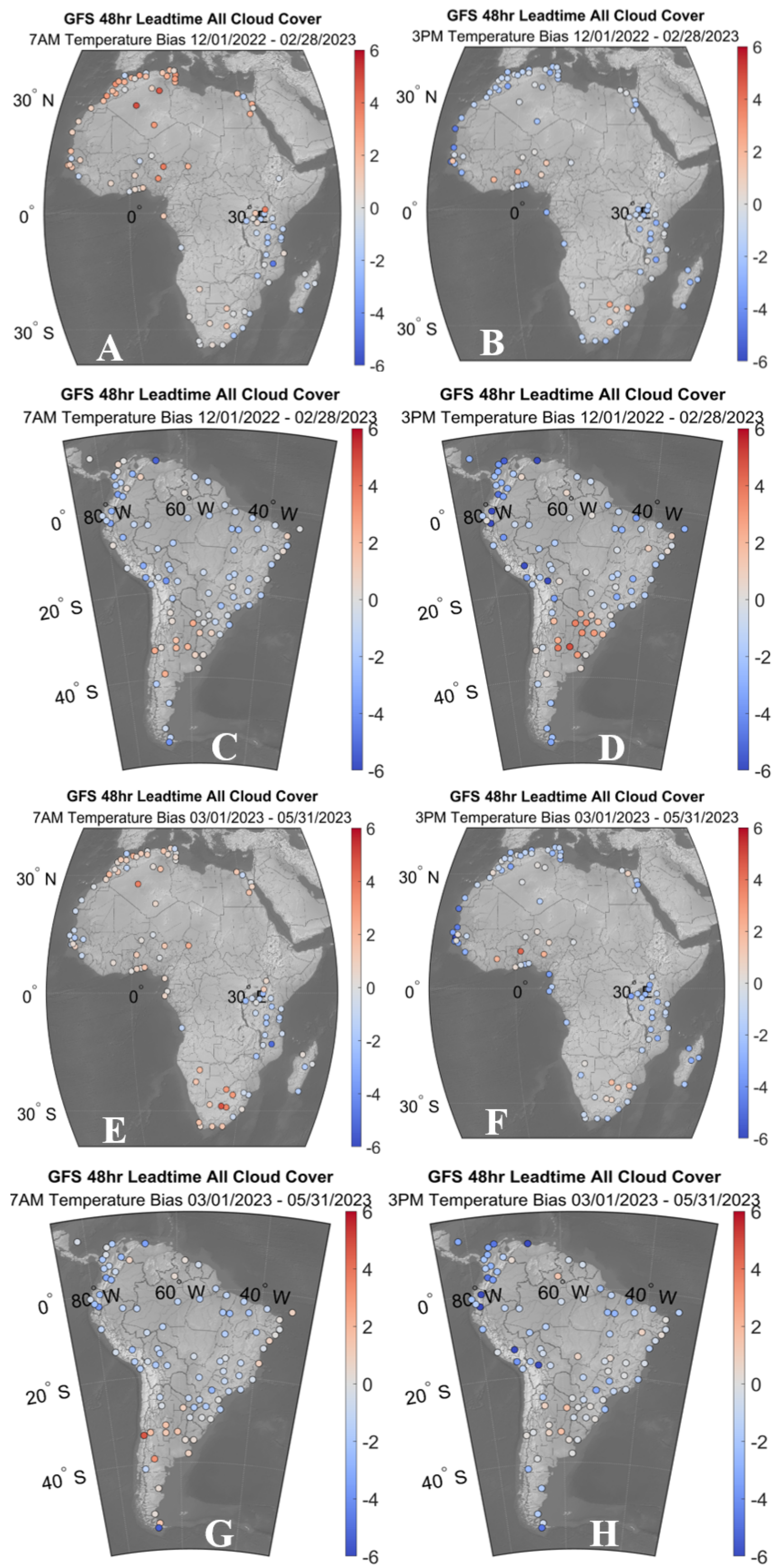

Figure 5.6: Geographical Map of Median Temperature Biases for DJF and MAM seasons, 2023

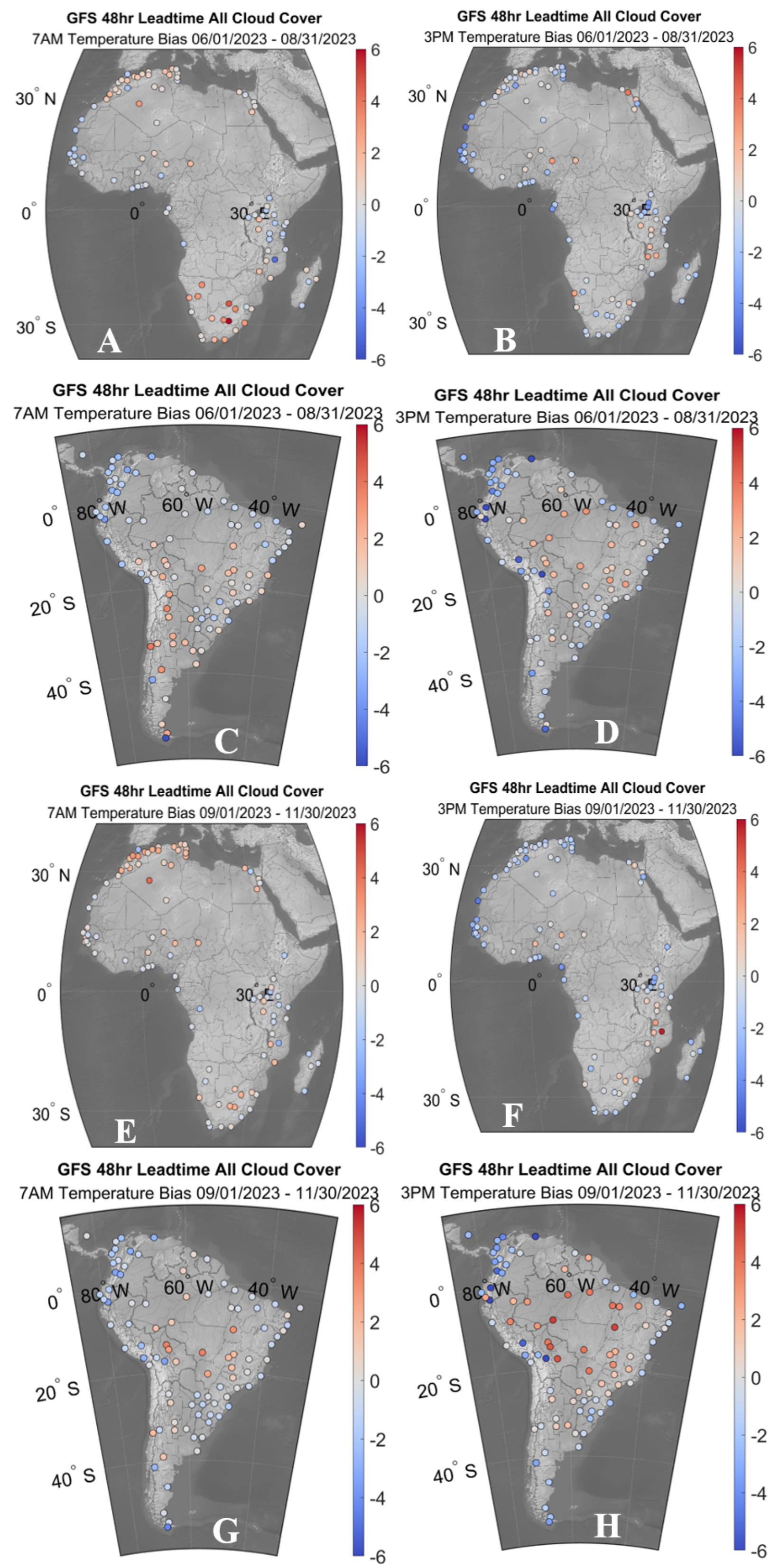

Figure 5.7: Geographical Map of Median Temperature Biases for JJA and SON seasons, 2023

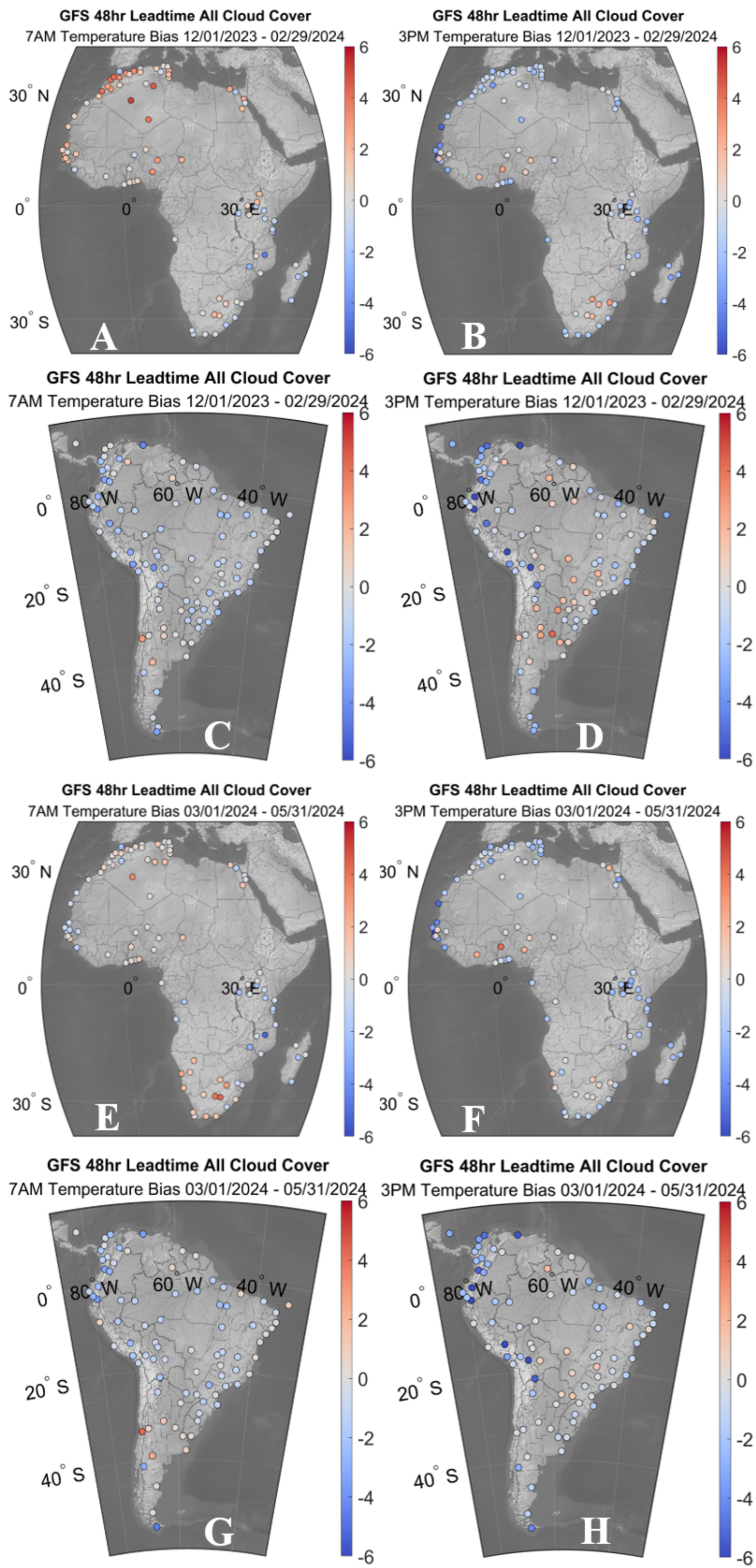

Figure 5.8: Geographical Map of Median Temperature Biases for DJF and MAM seasons, 2024

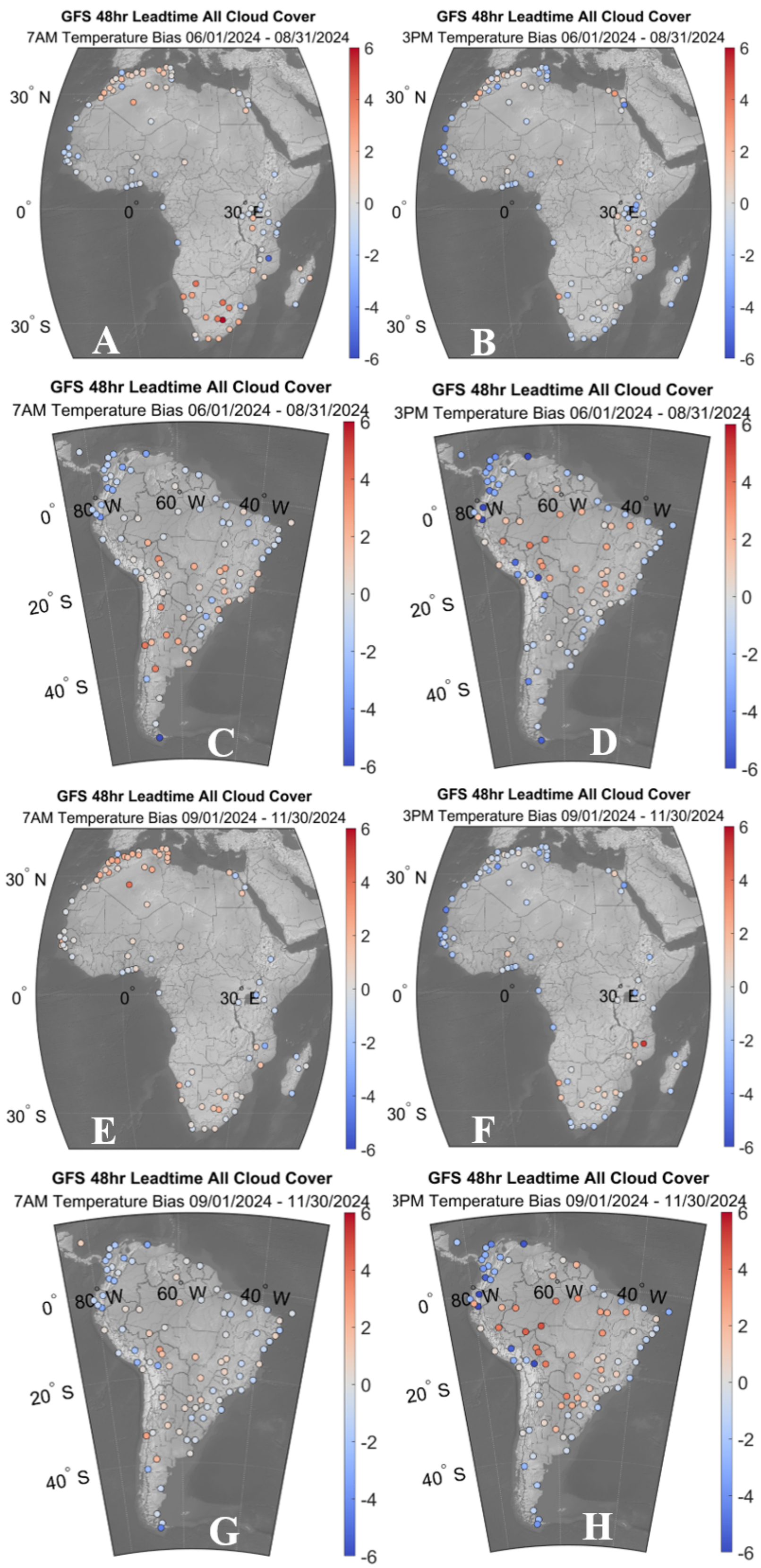

Figure 5.9: Geographical Map of Median Temperature Biases for JJA and SON seasons, 2024

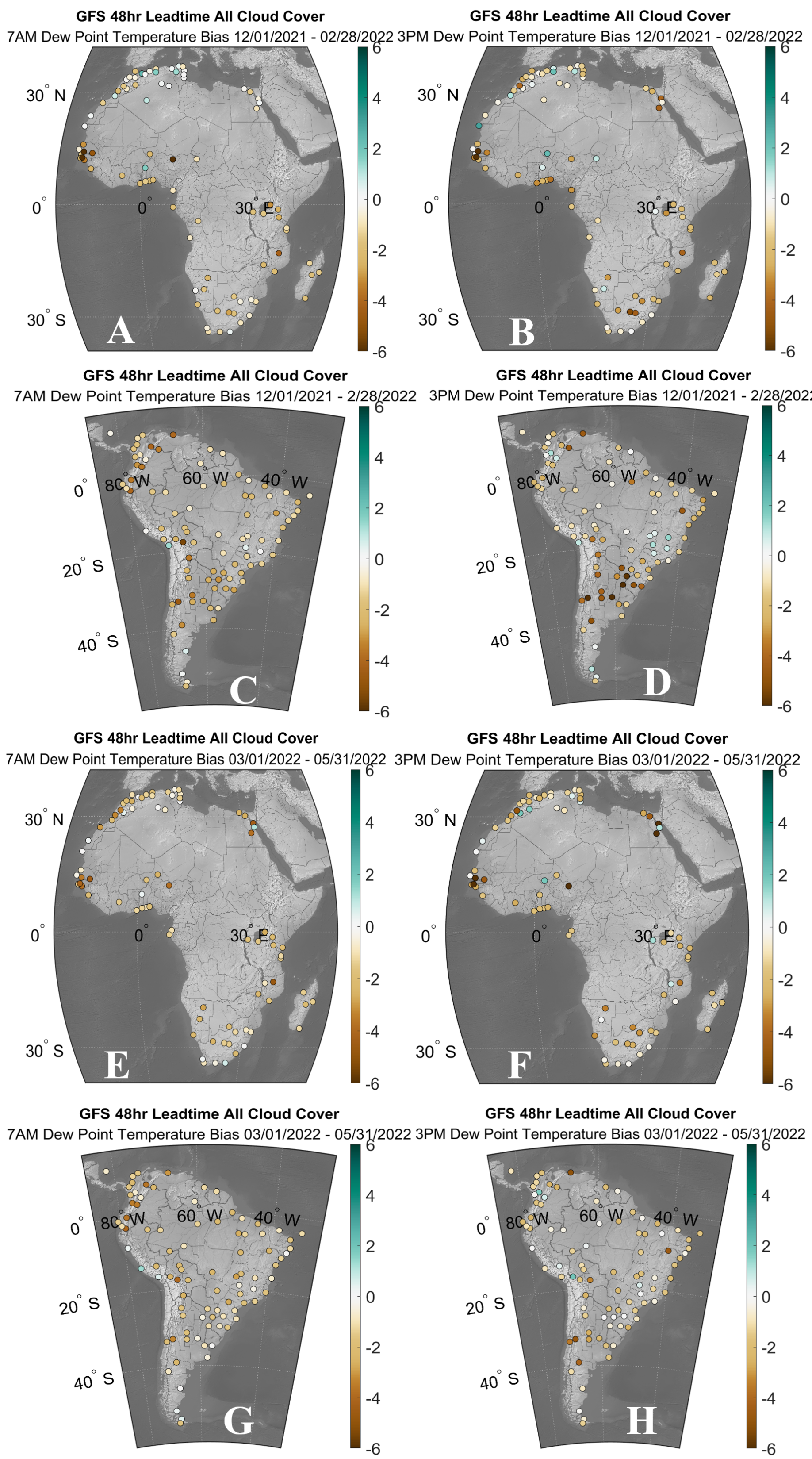

Figure 5.10: Geographical Map of Median Dewpoints Biases for DJF and MAM seasons, 2022

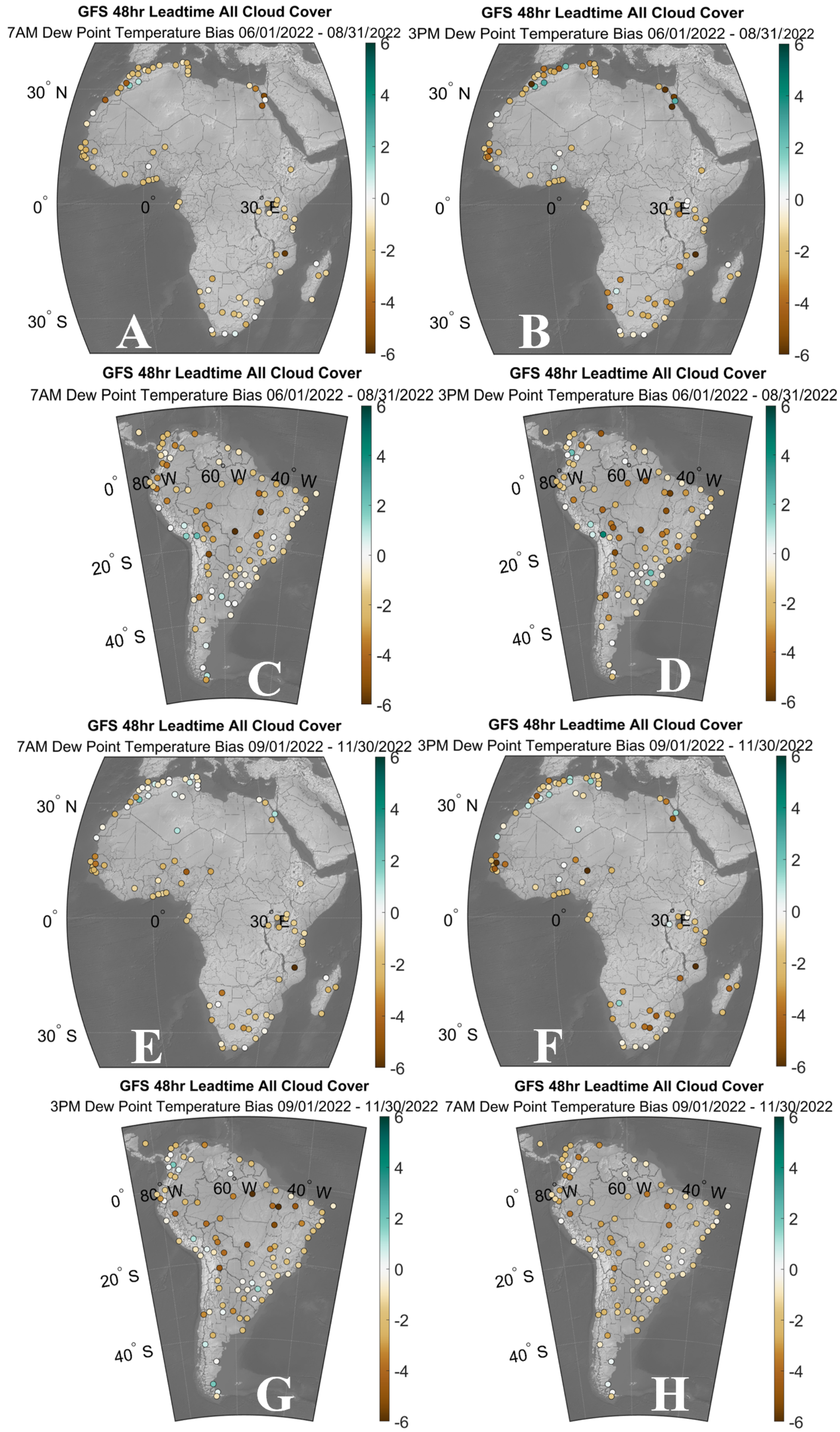

Figure 5.11: Geographical Map of Median Dewpoints Biases for JJA and SON seasons, 2022

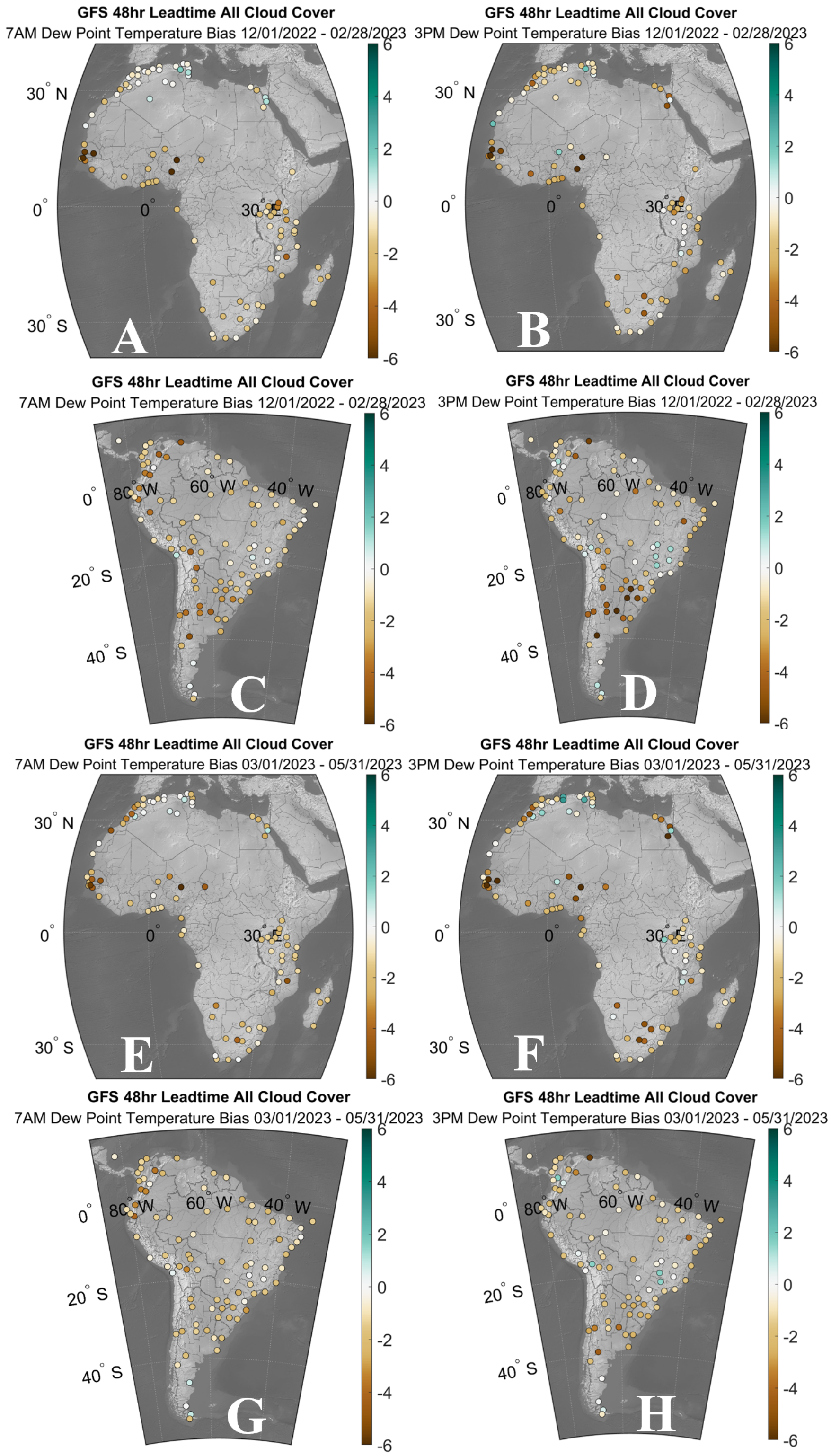

Figure 5.12: Geographical Map of Median Dewpoints Biases for DJF and MAM seasons, 2023

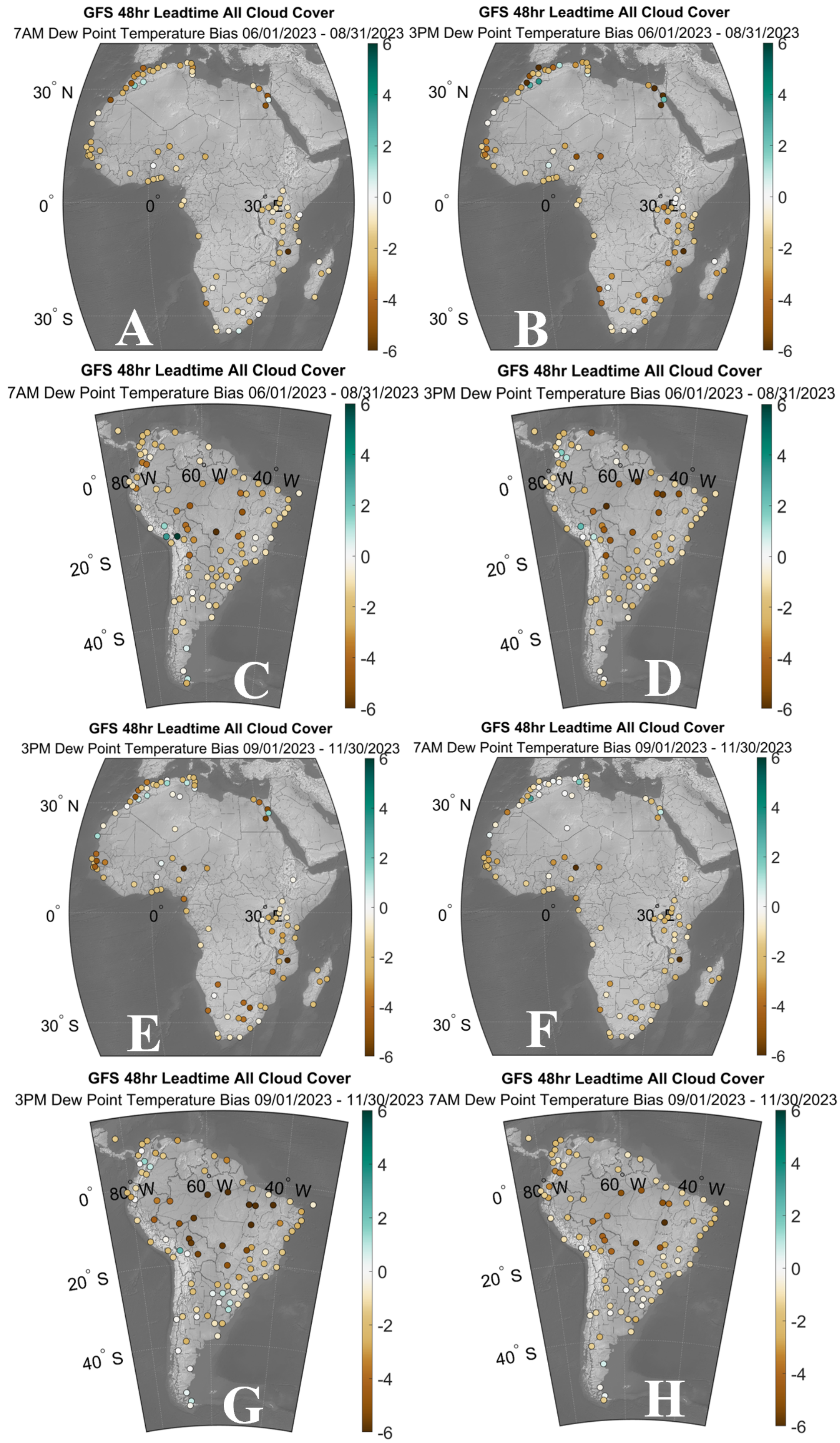

Figure 5.13: Geographical Map of Median Dewpoints Biases for JJA and SON seasons, 2023

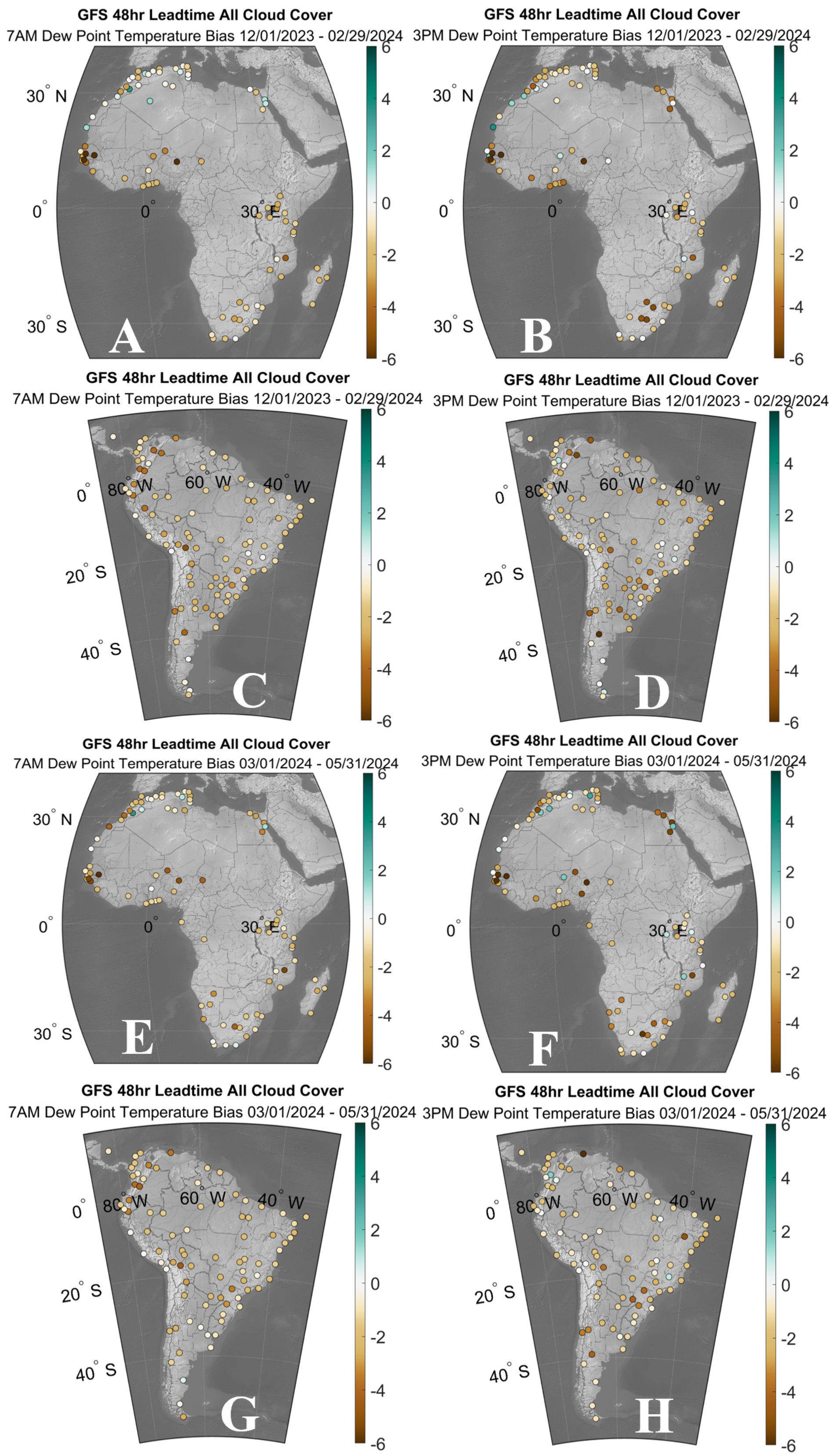

Figure 5.14: Geographical Map of Median Dewpoints Biases for DJF and MAM seasons, 2024

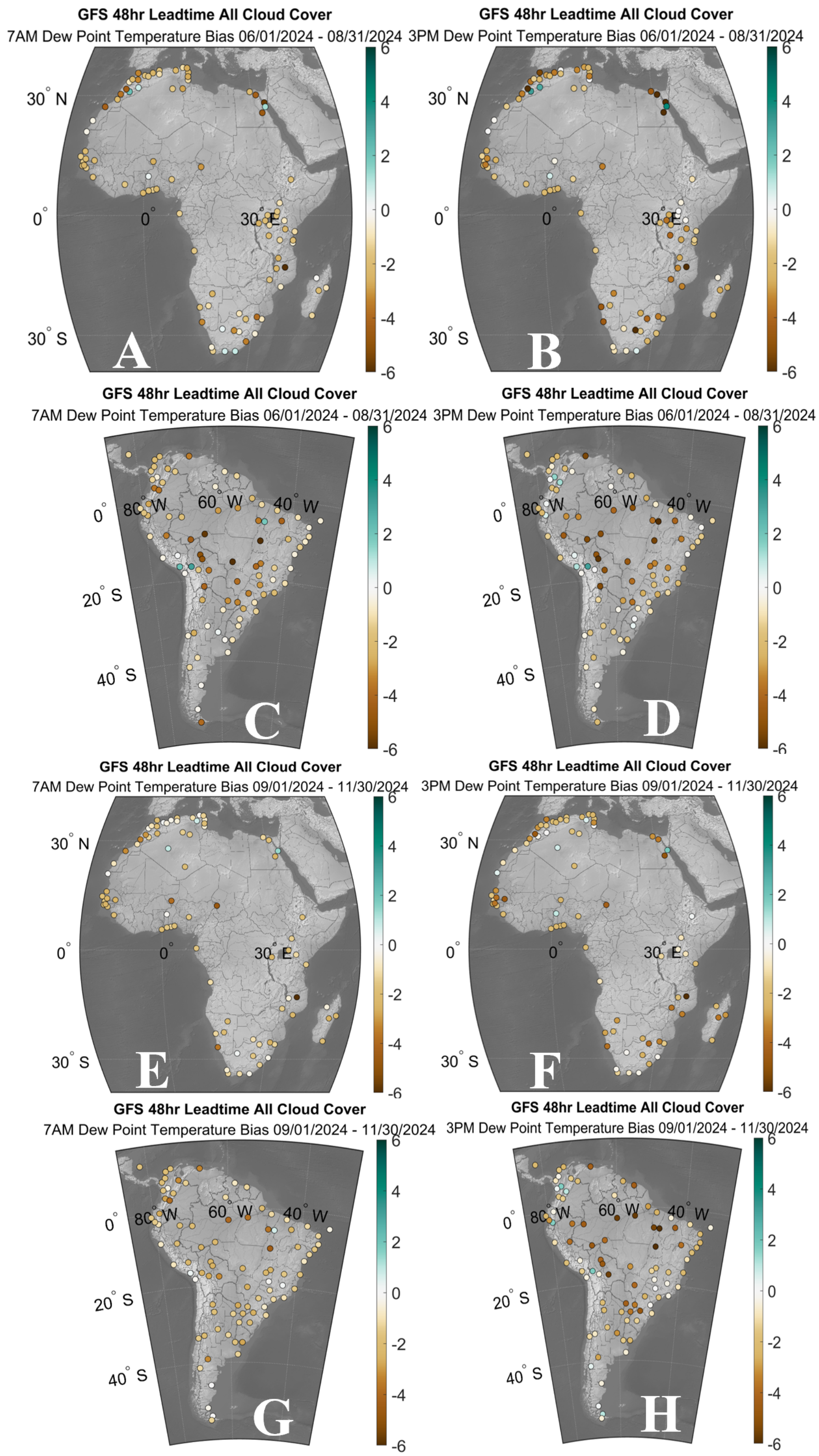

Figure 5.15: Geographical Map of Median Dewpoints Biases for JJA and SON seasons, 2024

Table 5.5: Summary statistics by climate zone for South America dew point bias including the 10th, 25th, 50th, and 90th percentiles. Under column for a 3-year period percentile average values (2022-2024). Highlighted in color are values with a median biases > ±1°C and 10th or 90th percentile biases > ±5°C.

Climate Zone	10th	25th	**50th**	75th	90th
Tropical 7am	-4.2	-2.3	**-1.6**	-1.1	-0.3
Tropical 3pm	**-5.2**	-3.2	**-1.8**	-0.5	0.6
Dry 7am	-4.1	-2.4	**-1.0**	0.2	1.6
Dry 3pm	**-5.4**	-3.3	**-1.7**	-0.3	1.3
Mediterranean 7am	-4.6	-3.1	**-1.6**	-0.1	1.4
Mediterranean 3pm	**-5.2**	-3.5	**-1.6**	0.2	2.1
Warm Wet Temperate 7am	-4.4	-2.9	**-1.6**	-0.3	0.9
Warm Wet Temperate 3pm	**-5.7**	-3.3	**-1.7**	-0.2	1.4
Cool Wet Temperate 7am	-4.7	-3.3	**-1.7**	-0.3	1.2
Cool Wet Temperate 3pm	-3.6	-2.2	**-0.4**	1.3	3.0